

Alcohol-abuse drug disulfiram targets cancer via p97 segregase adaptor NPL4

Zdenek Skrott^{1*}, Martin Mistrik^{1*}, Klaus Kaae Andersen², Søren Friis², Dusana Majera¹, Jan Gursky¹, Tomas Ozdian¹, Jirina Bartkova^{2,3}, Zsafia Turi¹, Pavel Moudry¹, Marianne Kraus⁴, Martina Michalova¹, Jana Vaclavkova¹, Petr Dzubak¹, Ivo Vrobel¹, Pavla Pouckova⁵, Jindrich Sedlacek⁶, Andrea Miklovcova⁷, Anne Kutt², Jing Li⁸, Jana Mattova⁵, Christoph Driessen⁴, Q. Ping Dou^{9,10}, Jørgen Olsen², Marian Hajduch¹, Boris Cvek^{6†}, Raymond J. Deshaies^{8,11†} & Jiri Bartek^{2,3}

Cancer incidence is rising and this global challenge is further exacerbated by tumour resistance to available medicines. A promising approach to meet the need for improved cancer treatment is drug repurposing. Here we highlight the potential for repurposing disulfiram (also known by the trade name Antabuse), an old alcohol-aversion drug that has been shown to be effective against diverse cancer types in preclinical studies. Our nationwide epidemiological study reveals that patients who continuously used disulfiram have a lower risk of death from cancer compared to those who stopped using the drug at their diagnosis. Moreover, we identify the ditiocarb-copper complex as the metabolite of disulfiram that is responsible for its anti-cancer effects, and provide methods to detect preferential accumulation of the complex in tumours and candidate biomarkers to analyse its effect on cells and tissues. Finally, our functional and biophysical analyses reveal the molecular target of disulfiram's tumour-suppressing effects as NPL4, an adaptor of p97 (also known as VCP) segregase, which is essential for the turnover of proteins involved in multiple regulatory and stress-response pathways in cells.

Despite advances in the understanding of cancer biology, malignant diseases have a high global toll. Furthermore, the increasing average human life expectancy is predicted to have demographic consequences, including an increase in the incidence of cancer. The high cancer-associated morbidity and mortality highlight the need for innovative treatments. Given the high costs, failure rate and long testing periods of developing new medicines, using drugs that are approved for the treatment of diverse diseases as candidate anti-cancer therapeutics represents a faster and cheaper alternative¹, benefitting from available clinically suitable formulations and evidence of tolerability in patients. Among promising cancer-killing drugs² is disulfiram (tetraethylthiuram disulfide, DSF), a drug that has been used for over six decades as a treatment for alcohol dependence³, with well-established pharmacokinetics, safety and tolerance at the US Food and Drug Administration (FDA)-recommended dosage⁴. In the body, DSF is metabolized to ditiocarb (diethylthiocarbamate, DTC) and other metabolites, some of which inhibit liver aldehyde dehydrogenase⁵. Because DSF showed anti-cancer activity in preclinical models^{3,6–9} and because adjuvant DTC was used to treat high-risk breast cancer in a clinical trial¹⁰, DSF emerges as a candidate for drug repurposing in oncology. Additional advantages of DSF include a broad spectrum of malignancies sensitive to DSF, and its ability to also target the stem-like, tumour-initiating cells¹¹. Although the mechanism of DSF's anti-cancer activity remains unclear and it has been suggested that the drug inhibits proteasome activity^{6,12}, it has been shown that DSF chelates bivalent metals and forms complexes with copper (Cu), which enhances its anti-tumour activity^{6,13}. In addition to the lack of a well-defined mechanism of action in cancer cells, the main obstacles for DSF repurposing have

been: (i) uncertainty about the active metabolite(s) of DSF *in vivo*; (ii) the lack of assays to measure these active derivative(s) in tumours; (iii) missing biomarker(s) to monitor the impact of DSF in tumours and tissues; (iv) the lack of insights into the preferential toxicity towards cancer cells compared to normal tissues; and (v) the absence of a specific molecular target that could explain the potent anti-tumour activity of DSF. Here, we combine experimental approaches and epidemiology to address the important characteristics of DSF in relation to cancer, pursuing the goal of repurposing DSF for cancer therapy. We identify the active metabolite of DSF, and provide biological validation and mechanistic insights, including the discovery of a biologically attractive protein that has previously not been considered as the target for the anti-cancer activity of DSF.

Epidemiological analyses of DSF and cancer

The relative lack of cancer-related clinical trials with DSF^{10,14} prompted us to explore whether DSF use might reduce cancer mortality at a population level. Using the Danish nationwide demographic and health registries, we estimated hazard ratios of cancer-specific mortality associated with DSF use among patients with cancer for the first time during 2000–2013 (see Methods, Table 1 and Extended Data Fig. 1a). DSF users were categorized as (i) previous users, who were patients that were prescribed DSF for alcohol dependency only before their cancer diagnosis or (ii) continuing users, who were patients that were prescribed DSF both before and after diagnosis. As expected from the increase in cancer risk and the deleterious effect on prognosis¹⁵ caused by alcohol abuse, cancer-specific mortality was higher among previous DSF users than among patients with cancer who had never

¹Institute of Molecular and Translational Medicine, Faculty of Medicine and Dentistry, Palacky University, Olomouc, Czech Republic. ²Danish Cancer Society Research Center, DK-2100 Copenhagen, Denmark. ³Science for Life Laboratory, Division of Genome Biology, Department of Medical Biochemistry and Biophysics, Karolinska Institute, Stockholm, Sweden. ⁴Kantonsspital St Gallen, Department Oncology/Hematology, St Gallen, Switzerland. ⁵Institute of Biophysics and Informatics, First Faculty of Medicine, Charles University, 120 00 Prague 2, Czech Republic. ⁶Department of Cell Biology & Genetics, Palacky University, Olomouc, Czech Republic. ⁷Psychiatric Hospital, 785 01 Šternberk, Czech Republic. ⁸Division of Biology and Biological Engineering, Caltech, Pasadena, California 91125, USA. ⁹Barbara Ann Karmanos Cancer Institute and Department of Oncology, School of Medicine, Wayne State University, Detroit, Michigan, USA. ¹⁰School of Basic Medical Sciences, Affiliated Tumor Hospital of Guangzhou Medical University, Guangzhou 511436, China. ¹¹Howard Hughes Medical Institute, Caltech, Pasadena, California 91125, USA. [†]Present addresses: Olomouc University Social Health Institute, Palacky University, Olomouc, Czech Republic (B.C.); Amgen, Thousand Oaks, California 91320, USA (R.J.D.).

*These authors contributed equally to this work.

Table 1 | Cancer-specific mortality associated with DSF use among Danish patients with cancer

Cancer type	Overall				Localized stage				Non-localized stage				Unknown stage			
	Number*	HR	95% CI	P value	Number*	HR	95% CI	P value	Number*	HR	95% CI	P value	Number*	HR	95% CI	P value
Any cancer†																
Previous users	3,038	1.00			1,429	1.00			1,054	1.00			555	1.00		
Continuing users	1,177	0.66	0.58–0.76	0.000	602	0.69	0.64–0.74	0.000	355	0.71	0.59–0.87	0.001	220	0.65	0.57–0.75	0.000
No prescriptions	236,950	0.68	0.64–0.73	0.000	113,354	0.59	0.57–0.61	0.000	73,933	0.80	0.73–0.88	0.000	49,663	0.66	0.62–0.71	0.000

Hazard ratios (HR) and 95% confidence intervals (CI) comparing continuing and previous users of DSF, relative to the time of their cancer diagnosis. For DSF exposure categories, statistics and clinical stages, see Methods.

*Number of patients included.

†Except cancers of the liver and kidney.

used DSF. Notably, we also found reduced cancer-specific mortality for cancer overall (Table 1), as well as for cancers of the colon, prostate and breast among continuing users compared to previous DSF users (Extended Data Fig. 1a). Stratification by clinical stage (Table 1) revealed reduced cancer-specific mortality with continuing use of DSF even among patients with metastatic disease. Although it is not possible to draw conclusions about causality, these findings supported the hypothesis that DSF may exert anti-cancer effects among patients suffering from common cancers, prompting us to perform pre-clinical analyses.

Anti-tumour activity of the DTC–copper complex

Because DSF anti-cancer activity has been suggested to be copper-dependent^{6,13}, we compared groups of mice injected with human MDA-MB-231 cancer cells, fed with a (i) normal diet; (ii) normal diet plus copper gluconate (CuGlu); (iii) normal diet plus DSF; or (iv) normal diet plus DSF and CuGlu (DSF/CuGlu); and tumour volume was measured over time (Fig. 1a and Extended Data Fig. 1b, c). Compared to matched controls, tumour volume in DSF- and DSF/CuGlu-treated groups at 32 days (at DSF doses equivalent to those used by alcoholics) were suppressed by 57% and 77%, respectively ($P = 0.0038$ in favour of the DSF/CuGlu treatment versus DSF alone). These results validate previous *in vitro*^{6,11,13} and *in vivo*^{6–9,13,16} studies, which indicated that DSF is an efficient anti-cancer agent and that copper potentiates its activity. As the reactive metabolite DTC forms complexes with metals, particularly copper¹⁷, we argued that a DTC–copper complex (bis (diethyldithiocarbamate)–copper (CuET)) forms *in vivo* (Extended Data Fig. 1d), providing the anti-cancer metabolite. To test this hypothesis, we developed a high-resolution

approach based on high-performance liquid chromatography–mass spectrometry to measure CuET in tissues, and readily detected CuET after a single oral dose of DSF (Extended Data Fig. 1e, f). Extracts from plasma, liver, brain and MDA-MB-231-xenografted tumours contained CuET in samples from mice treated for five days with DSF or DSF/CuGlu. The CuET levels in plasma and liver were slightly higher after DSF/CuGlu treatment compared to DSF alone. Notably, the CuET levels in the tumour specimens were almost an order of magnitude higher compared to corresponding levels in liver and brain tissues from the same animals (Fig. 1b), suggesting preferential accumulation of CuET in tumours. Importantly, we also confirmed formation of CuET in humans undergoing DSF treatment for alcoholism (Fig. 1c).

Next, we synthesized CuET and performed comparative cell culture and animal studies. Short-term (24-h) assays and long-term (colony-forming assay, CFA) assays consistently showed higher cytotoxicity of CuET than of the primary DSF metabolite DTC in various cancer cell lines (Fig. 1d and Extended Data Fig. 1g). The half-maximal lethal dose (LD_{50}) values of CuET in CFA experiments were ≤ 100 nM in three out of three tested breast cancer cell lines and similar potency was observed among cell lines derived from human lung, colon and prostate tumours (Extended Data Fig. 2a). These data were corroborated by tetrazolium dye ((2,3-bis-(2-methoxy-4-nitro-5-sulphophenyl)-2h-tetrazolium-5-carboxanilide) (XTT))-based 48-h cytotoxicity tests on a wider panel of cell types (Extended Data Fig. 2b). Unexpectedly, only the most sensitive cell lines (for example, AMO-1, Capan1) showed markers of apoptosis¹⁸, which included annexin V and activated caspases, whereas in most cell lines, for example, MDA-MB-231 and U2OS cells, CuET induced apoptosis-independent cell death (Extended Data Fig. 2c–f).

Direct therapeutic effects of CuET *in vivo* were then investigated using the MDA-MB-231 breast cancer (Fig. 1e) and AMO-1 myeloma (Fig. 1f) xenograft models treated intraperitoneally with a CuET–albumin formulation, with which the anti-tumour activity and good tolerability of this DSF metabolite was confirmed (Extended Data Fig. 1h, i).

CuET inhibits p97-dependent protein degradation

Next, we investigated the interaction between CuET and cellular protein degradation, one of the suggested explanations for anti-tumour effects of DSF^{6,12}. We confirmed that CuET induces phenotypic features shared with proteasome inhibitors, such as MG132 or bortezomib (BTZ), including accumulation of poly-ubiquitylated (poly-Ub) proteins (Fig. 2a and Extended Data Fig. 3a), rapid deubiquitylation of ubiquitylated proteins in the cytoplasm¹⁹ (Extended Data Fig. 3c). Furthermore, TNF (also known as TNF α)-induced degradation of I κ B α (ref. 20) was blocked after 1-h treatment with CuET or BTZ (Fig. 2b). Finally, CuET inhibited degradation of Ub(G76V)–GFP (an ubiquitin-fusion degradation substrate)²¹ in a dose-dependent manner (Fig. 2c). However, although these data confirmed a defect in protein degradation, CuET had no effect on the CT-like, C-like or T-like activity of the 20S proteasome²² (Extended Data Fig. 3d, e). This was further corroborated by the lack of a stabilizing effect of CuET on p53 tumour suppressor protein in dicoumarol-treated cells, in which

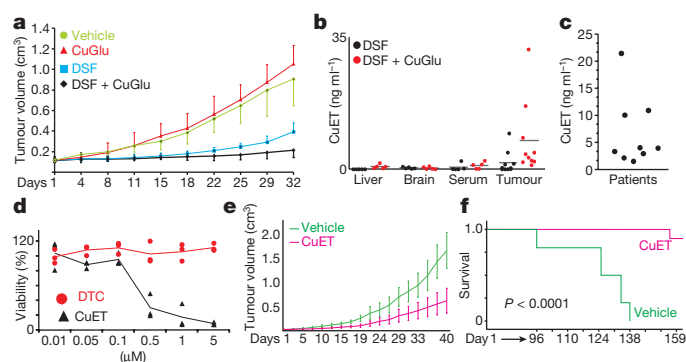


Figure 1 | Tumour-suppressing effects of DSF and CuET. **a**, Effects of orally administered DSF and CuGlu on subcutaneous growth of MDA-MB-231 tumours in mice. $n = 8$ mice per group. **b**, CuET levels in mouse tumours and tissues. $n = 5$ tissues, $n = 10$ tumours. **c**, CuET levels in human plasma after DSF treatment ($n = 9$ patients). **d**, Toxicity of DTC and CuET in MDA-MB-231 cells after 24 h treatment. $n = 3$ experiments. **e**, Effect of CuET on subcutaneous growth of MDA-MB-231 tumours in mice. $n = 20$ tumours. **f**, Survival of CuET- versus vehicle-treated mice with implanted AMO-1 xenografts. $n = 10$ animals per group. P value from a log-rank test. Data are mean \pm s.d. (**a**, **e**) or mean (**b**) linked means with individual values (**d**) or individual values (**c**).

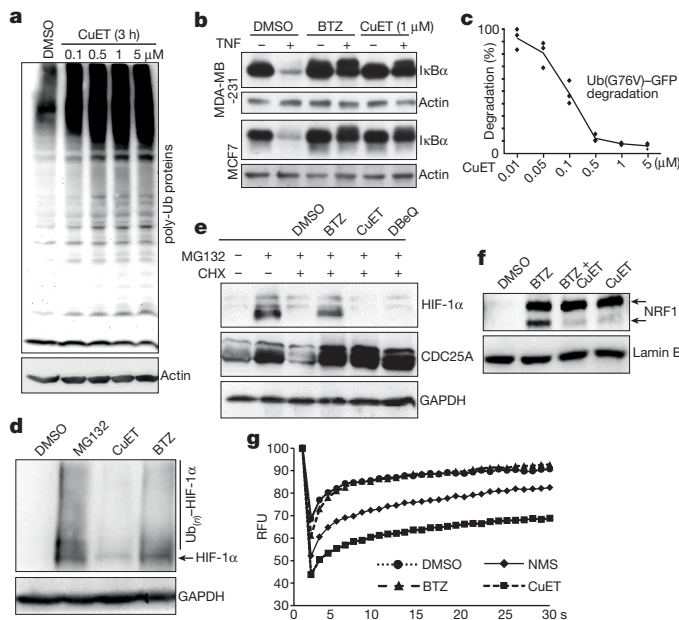


Figure 2 | CuET inhibits p97 segregase-dependent protein degradation. **a**, CuET causes accumulation of poly-ubiquitylated proteins in MCF7 cells. **b**, TNF-induced I κ B α degradation is compromised after 1-h treatment with CuET or BTZ. **c**, Dose-dependent inhibition of Ub(G76V)-GFP degradation by CuET. HeLa cells were treated for 3 h. $n = 3$ experiments. **d**, HIF-1 α levels after 2-h treatments with MG132 (5 μ M), CuET (1 μ M), BTZ (1 μ M) in HeLa cells. **e**, Differential effect of BTZ (1 μ M), CuET (1 μ M) and DBEQ (10 μ M) on CDC25A versus HIF-1 α in MG132-pretreated (4 h, 5 μ M), cycloheximide (CHX, 1 h, 50 μ g ml $^{-1}$)-exposed HeLa cells. **f**, BTZ (8 h, 1 μ M) induces NRF1 120-kDa (top arrow) and 110-kDa (bottom arrow) forms; whereas CuET (8 h, 0.5 μ M) only induced the non-cleaved 120-kDa form in NIH3T3 cells. **g**, FRAP quantification in U2OS Ub-GFP cells: slower mobility of accumulated cytoplasmic GFP-Ub after a 2-h pre-treatment with NMS873 (10 μ M), CuET (1 μ M) or BTZ (1 μ M). **a**, **b**, **d**-**g**, Data are representative of two independent biological experiments. Data are linked means and individual values (**c**) and relative mean signal of the bleached region from 12 cells per treatment (**g**).

p53 turnover depends on the core 20S proteasome independently of ubiquitin^{23,24}. In contrast to CuET, treatment with the 20S proteasome inhibitor BTZ stabilized p53 irrespective of dicoumarol (Extended Data Fig. 3f), indicating that 20S proteasome-dependent protein turnover remains operational with CuET treatment. Furthermore, CuET failed to inhibit 26S proteasome activity (Extended Data Fig. 3g), which was inferred from RPN11-dependent deubiquitylation²⁵. Collectively, these results suggest that CuET stabilizes ubiquitylated proteins by blocking a step upstream of the proteasome.

Next we considered p97-dependent processing of poly-Ub proteins, as this pathway operates upstream of the proteasome and its malfunction resembles phenotypes of proteasome inhibition²⁶. Unlike BTZ or MG132, CuET induced only modest accumulation (a small subfraction) of HIF-1 α (Fig. 2d), consistent with reported modest accumulation of HIF-1 α after knockdown of p97 compared to cells with inhibited proteasomes²⁷. Next, we pre-treated cells with MG132, followed by wash-off and 1-h cycloheximide (an inhibitor of translation) treatment combined with BTZ, CuET or DBEQ (a direct inhibitor of p97 ATPase activity)²⁸. All tested inhibitors prevented degradation of CDC25A (a known p97 target)²⁹, whereas degradation of the mostly p97-independent target, that is, most of HIF-1 α ²⁷, was inhibited only by BTZ (Fig. 2e). Furthermore, consistent with cleavage of the 120-kDa species of the endoplasmic reticulum-tethered transcription factor NRF1 into an active 110-kDa form being a p97-dependent process³⁰, appearance of the cleaved NRF1 form was inhibited by both CuET and NMS873 (another p97 ATPase inhibitor) (Fig. 2f and Extended Data Fig. 4a, b).

These results suggest that the p97 pathway is compromised in cells treated with CuET.

Next, we asked whether CuET impairs the p97 segregase activity that extracts poly-Ub proteins from cellular structures, such as the endoplasmic reticulum, Golgi apparatus or chromatin for subsequent proteasomal degradation³¹. Using fluorescence recovery after photobleaching (FRAP) to investigate the mobility of accumulated poly-Ub proteins, we found that whereas GFP-ubiquitin in DMSO- or BTZ-treated cells diffused rapidly into bleached areas, this diffusion was slower after treatment with CuET or NMS873 (Fig. 2g and Extended Data Fig. 4c). This suggests that after treatment with CuET or NMS873 at least a subset of the accumulated poly-Ub proteins remains immobile, probably embedded into cellular structures. Consistently, upon detergent pre-extraction of mobile proteins, we observed greater immunofluorescence signals of extraction-resistant poly-Ub(K48) proteins (destined for proteasomal degradation) in NMS873- and CuET-treated cells compared to BTZ- or DMSO-treated controls (Extended Data Fig. 4d). Western blot analysis of endoplasmic reticulum-rich microsomal fractions also revealed enrichment of poly-Ub proteins after CuET and NMS873 treatment (Extended Data Fig. 4e). Malfunction of p97 segregase is furthermore associated with a cellular unfolded protein response (UPR)³². We confirmed UPR in cells treated with CuET or NMS873 by detecting increased markers of UPR induction, including the spliced form of XBP1s, ATF4 and phosphorylated (p-) eIF2 α ³³ (Extended Data Fig. 4f).

These studies are also of clinical relevance, because inhibition of p97 was suggested as an alternative treatment strategy for myeloma patients who had relapsed after therapy with BTZ (also known by the trade name Velcade)³⁴ or carfilzomib (CFZ)³⁵. Thus, we performed cytotoxicity tests with CuET on a panel of BTZ- or CFZ-adapted and non-adapted human cell lines or on cells derived from samples of patients with myeloma before therapy and with BTZ therapy. All pairs of adapted and non-adapted cells showed similar sensitivity to CuET treatment, in contrast to BTZ (Extended Data Fig. 5a-d). These results suggest that treatment with DSF (best combined with copper) or CuET might become a feasible therapeutic option for patients with relapsed, BTZ-resistant multiple myeloma.

CuET binds and immobilizes NPL4

To elucidate how CuET inhibits the p97 pathway, we first used an assay of p97 ATPase activity²⁸. In contrast to treatment with NMS873, CuET had no effect on p97 ATPase activity (Extended Data Fig. 6a). Because NPL4 and UFD1 proteins are key components of the p97 segregase³¹, we examined whether CuET might target the pathway through these cofactors. Ectopic overexpression of NPL4-GFP, but not UFD1-GFP or p97-GFP, reduced CuET cytotoxicity, suggesting that NPL4 is a candidate target of CuET (Fig. 3a and Extended Data Fig. 6b). An analogous 'rescue effect' of ectopic NPL4-GFP was apparent from the reduction in accumulation of poly-Ub proteins caused by CuET (Extended Data Fig. 6c).

As shown by live-cell imaging, 2-3-h exposure to CuET induced prominent nuclear clustering of NPL4-GFP, but not of UFD1-GFP or p97-GFP (Fig. 3b). Within 2-3 h, most of cellular NPL4-GFP became immobilized in nuclear clusters and also in cytoplasmic areas, as shown by FRAP (Fig. 3c). CuET-induced immobilization of endogenous NPL4 was confirmed by accumulation, which was detectable by western blot, in the detergent-insoluble fractions from various cell lines (Fig. 3d) and by immunofluorescence on pre-extracted cells (Extended Data Fig. 6d). Notably, the immobilization of NPL4 was also detectable in pre-extracted sections of cryopreserved tumours from mice treated with DSF or DSF and CuGlu, thus providing a potential biomarker of CuET activity towards the p97 pathway *in vivo* (Fig. 3e).

NPL4 is an attractive candidate for CuET binding, because this protein contains two zinc finger domains: a C-terminal NZF (NPL4-zinc finger) and a putative zinc finger-NPL4³⁶, which bind bivalent metals and metal complexes that might chemically resemble CuET³⁷.

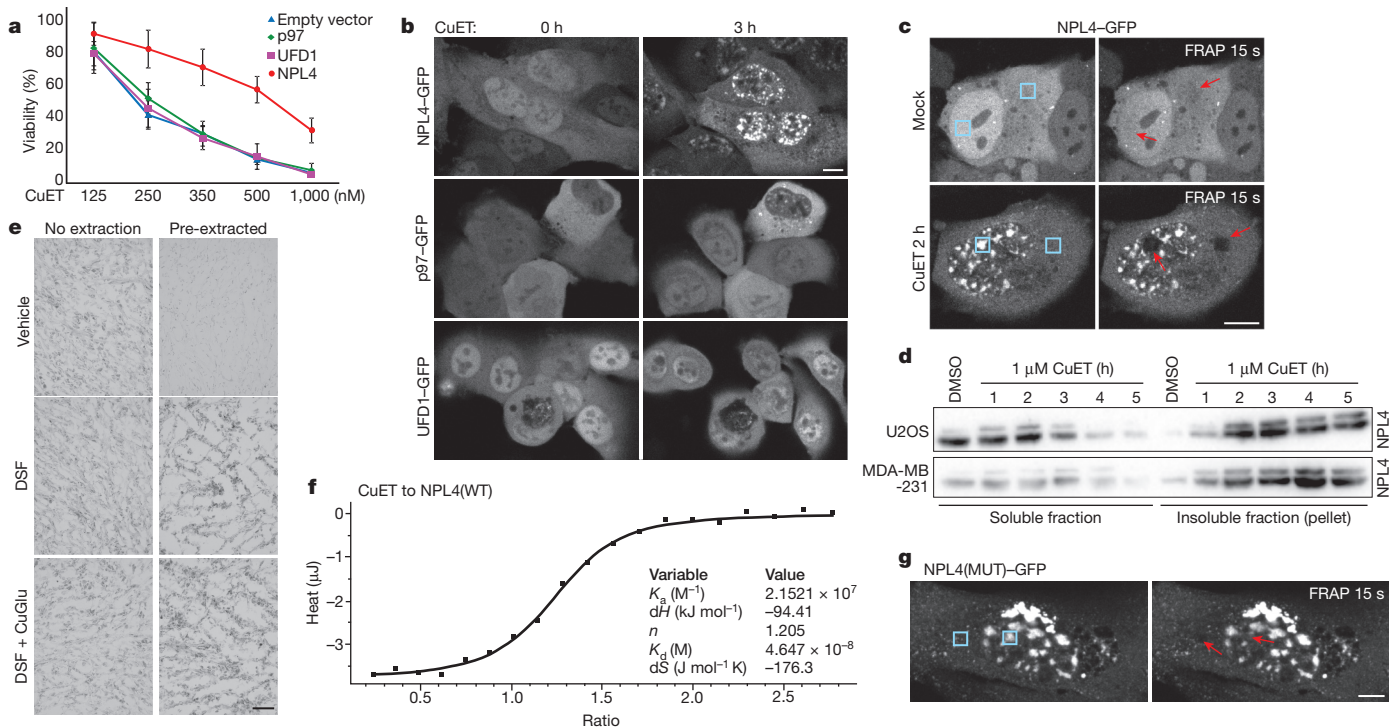


Figure 3 | CuET binds to and immobilizes NPL4. **a**, Ectopic NPL4-GFP, but not p97-GFP or UFD1-GFP rescues CuET toxicity in U2OS cells treated for 24 h. $n = 3$ experiments. Data are mean \pm s.d. **b**, CuET (1 μ M) induces intranuclear clustering of NPL4-GFP, but not p97-GFP or UFD1-GFP. **c**, CuET-induced (1 μ M) immobilization of NPL4-GFP (FRAP) in U2OS cells treated for 2 h. Blue boxes, areas before bleaching; arrows, after bleaching. **d**, NPL4 enrichment in Triton X-100-insoluble fractions

after CuET (1 μ M) treatment. **e**, Immunohistochemistry demonstrates the non-extractable NPL4 in MDA-MB-231 tumours from mice treated with DSF or DSF and CuGlu. **f**, ICT shows that CuET binds to purified NPL4(WT). **g**, Spontaneous intranuclear clustering and immobilization of NPL4(MUT)-GFP using FRAP in U2OS cells. Blue boxes, areas before bleaching; arrows, after bleaching. Scale bars, 10 μ m (**b**, **c**, **g**) or 50 μ m (**e**). **b-g**, Data are representative of two independent experiments.

Using isothermal calorimetry analysis (ITC)³⁸, we observed a standard dose-response-dependent binding curve (Fig. 3f) compatible with one binding site for CuET on wild-type NPL4 (NPL4(WT)), and a K_d in nanomolar concentrations for the NPL4-CuET interaction. Next, we used mutagenesis to test whether the putative ZF-NPL4 domain has any role in the potential NPL4-CuET interaction. The putative zinc finger domain was preferred, because an endogenous larger form of NPL4 that lacks the C-terminal NZF sequence exists in human cells. This larger NPL4 form is detectable as an upper band on western blots (Fig. 3d) and it is immobilized after CuET treatment, suggesting that the C-terminal NZF is not necessary for the interaction with CuET. No ITC interaction was found with a NPL4 mutant (NPL4(MUT)) (Extended Data Fig. 6f) in which both histidines and both cysteines in the putative zinc finger domain were substituted by alanines (Extended Data Fig. 6e). We used drug affinity responsive target stability (DARTS) as another, independent approach, which is based on altered protease susceptibility of target proteins upon drug binding³⁹. Consistently, exposure to CuET caused a differential pronase-dependent proteolysis pattern of NPL4(WT) but not NPL4(MUT) (Extended Data Fig. 6g). These results indicate that NPL4 is directly targeted by CuET and an intact putative zinc finger domain of NPL4 is essential for this interaction.

Notably, ectopically expressed NPL4(MUT)-GFP formed immobile nuclear clusters spontaneously in untreated cells, reminiscent of events seen in cells upon CuET treatment (Fig. 3c, g). Moreover, unlike ectopic NPL4(WT)-GFP, ectopically expressed NPL4(MUT)-GFP not only did not render cells resistant to CuET but also was toxic to the acceptor cells (Extended Data Fig. 6h). We also confirmed that multiple CuET-induced cellular phenotypes were mimicked by the ectopic NPL4(MUT)-GFP model, including accumulation of poly-Ub proteins and UPR activation (Extended Data Fig. 6i).

NPL4 aggregates trigger a heat-shock response

Although the nuclear NPL4 clusters occupied DAPI-unlabelled areas of chromatin (Extended Data Fig. 6d) co-localization with DAPI-excluded structures, such as nucleoli and nuclear speckles, were not found (Extended Data Fig. 7a). In late-G2 cells, NPL4 clusters were evidently excluded from the partially condensed chromatin (Extended Data Fig. 7b), suggesting that the NPL4 aggregates exclude chromatin rather than accumulating in specific nuclear areas. Both the nuclear clusters and the immobilized cytoplasmic NPL4 co-localized with poly-Ub proteins (confirmed by anti-Ub(K48) and FK2 antibodies), small ubiquitin-like modifiers (SUMOs) (only in nuclei) and with TDP43 protein⁴⁰ (Fig. 4a and Extended Data Fig. 7d), which are all features typical of aggregated defective proteins⁴¹. The same co-localization patterns were observed for spontaneous clusters formed by NPL4(MUT)-GFP showing that NPL4 aggregation is sufficient for the induction of these phenotypes even without CuET treatment (Extended Data Fig. 7c, e). Blockade of cellular ubiquitylation with a chemical inhibitor (MLN7243) of the E1 ubiquitin-activating enzyme failed to prevent either NPL4-GFP nuclear aggregation or cytoplasmic immobilization (Extended Data Fig. 7d), excluding the immobilization of NPL4 via recognition of ubiquitylated and SUMOylated substrates, but rather suggesting that immobilized NPL4 attracts ubiquitylated proteins or proteins that subsequently become ubiquitylated and/or SUMOylated. A key protein commonly associated with intracellular protein aggregates is HSP70, a chaperone implicated in aggregate processing⁴². Indeed, pre-extracted cells showed co-localization of HSP70 with both CuET-induced NPL4(WT)-GFP and spontaneous NPL4(MUT)-GFP aggregates (Fig. 4b, c). Both the CuET-induced NPL4(WT) aggregates and spontaneous NPL4(MUT) aggregates also co-localized with p97 (Extended Data Fig. 7f, g), as is particularly evident after pre-extraction. In the NPL4-GFP model, the amount of p97 immunoreactivity within

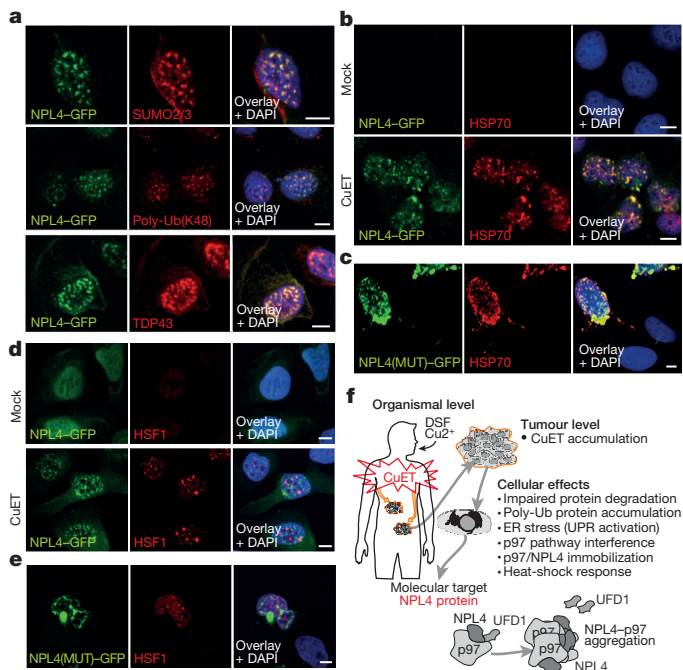


Figure 4 | NPL4 protein aggregation triggers HSR. a, NPL4–GFP co-localizes with SUMO2/3, poly-Ub(K48) and TDP43 in U2OS cells. Cells were treated with 1 μ M CuET for 3 h and pre-extracted. **b**, NPL4–GFP co-localizes with HSP70 in mock- and CuET-treated U2OS cells. Cells were treated with 1 μ M CuET for 3 h and pre-extracted. **c**, NPL4(MUT)–GFP co-localizes with HSP70 in U2OS cells after pre-extraction. **d**, CuET-induced HSF1 stress bodies. NPL4–GFP U2OS cells were treated with 1 μ M CuET for 3 h. **e**, HSF1 stress bodies in U2OS cells expressing NPL4(MUT)–GFP. **f**, Model of DSF anti-cancer activity in patients. Scale bars, 10 μ m. **a–e**, Data are representative of two independent experiments.

the NPL4–GFP clusters correlated with the GFP signal intensity, suggesting that p97 is immobilized via its interaction with NPL4. The other NPL4-binding partner, UFD1, was almost undetectable in detergent-insoluble pellets of CuET-treated or NPL4(MUT)–GFP-expressing cells despite clear p97 immobilization (Extended Data Fig. 8a, b), suggesting that UFD1 cannot bind to, or becomes only loosely attached to, the aggregated NPL4–p97 complex. Notably, non-extractable cellular p97 is detectable after CuET treatment (Extended Data Fig. 8c), including in stained tumour sections from mice treated with DSF or DSF and CuGlu, providing an additional candidate marker for CuET activity *in vivo* (Extended Data Fig. 8d).

Because aggregation of misfolded or damaged proteins triggers cellular heat-shock response (HSR) through an HSF1-dependent mechanism⁴³, we confirmed that CuET treatment indeed triggered a robust HSR accompanied by characteristic HSF1 nuclear stress foci (Fig. 4d) that were also detectable in cells spontaneously aggregating NPL4(MUT)–GFP (Fig. 4e). HSR markers, including accumulation of heat-shock proteins and a phosphorylation shift in HSF1, were detectable by western blot (Extended Data Fig. 8e, f).

Discussion

Our results help to explain the anti-cancer activity of the alcohol-abuse drug disulfiram. We propose a model for DSF cytotoxic activity, featuring rapid conversion of DSF into CuET, which accumulates in tumours. After entering cells, CuET binds NPL4 and induces its aggregation, consequently disabling the vital p97–NPL4–UFD1 pathway and inducing a complex cellular phenotype leading to cell death (Fig. 4f). Supporting CuET as the active metabolite is the correlation of CuET concentrations (active in the nanomolar range) with the biological effects and functional impact on the targeted pathway(s) *in vivo*. In addition, CuET is the only known metabolite of DSF containing copper ions, a metal

that enhances the anti-tumour effects of DSF; it is unlikely that another DSF metabolite could represent the major anti-cancer agent as levels of non-CuET metabolites should be lowered by copper addition. We also present a method for CuET detection in tissues and plasma, as well as data suggesting that preferential accumulation of CuET in tumours may contribute to cancer cell toxicity, consistent with the high therapeutic tolerability of DSF³, as documented even after years of daily administration at doses comparable to those we used in our mouse experiments. Considering the numerous studies on DSF and diverse opinions about the potential target of its anti-cancer effects⁴⁴, identification of NPL4, a key component of the p97–NPL4–UFD1 segregase complex, as the molecular target of CuET is surprising. The CuET–NPL4 interaction leads to rapid formation of protein aggregates and immobilization of this otherwise very mobile multifunctional protein complex, resulting in a severe phenotype, induction of HSR and eventually cell death. While additional potential targets of CuET cannot be excluded, the malfunction of the p97 pathway due to the NPL4–p97 aggregate formation explains the major cell phenotypes and the consequent cell death. Our work also reconciles the controversial studies^{6,12}, suggesting that the proteasome is the DSF target, by demonstrating that neither 20S nor 26S proteasome, but the processing of ubiquitylated proteins by the NPL4-dependent segregase, is targeted by CuET. Our results support the notion that the p97–NPL4 pathway is a promising therapeutic target in oncology^{45,46}. Indeed, reports on p97 overabundance correlating with progression and metastasis of carcinomas of the breast, colon and prostate^{47–49} are consistent with our present nationwide epidemiological analysis, which revealed an association between continued use of DSF and favourable prognosis, an intriguing finding that should be investigated further, particularly given the currently limited therapeutic options for patients with metastatic cancer. From a broader perspective, our study illustrates the potential of multifaceted approaches to drug repurposing, providing novel mechanistic insights, identification of new cancer-relevant targets and encouragement for further clinical trials, here with DSF, an old, safe and public domain drug⁴ that might help to save lives of patients with cancer worldwide.

Online Content Methods, along with any additional Extended Data display items and Source Data, are available in the online version of the paper; references unique to these sections appear only in the online paper.

Received 1 October 2015; accepted 8 November 2017.

Published online 6 December 2017.

- Collins, F. S. Mining for therapeutic gold. *Nat. Rev. Drug Discov.* **10**, 397 (2011).
- Pantziarka, P. *et al.* The repurposing drugs in oncology (ReDO) project. *Eur. J. Cancer* **50**, 442 (2014).
- Iljin, K. *et al.* High-throughput cell-based screening of 4910 known drugs and drug-like small molecules identifies disulfiram as an inhibitor of prostate cancer cell growth. *Clin. Cancer Res.* **15**, 6070–6078 (2009).
- Cvek, B. Nonprofit drugs as the salvation of the world's healthcare systems: the case of Antabuse (disulfiram). *Drug Discov. Today* **17**, 409–412 (2012).
- Shen, M. L., Johnson, K. L., Mays, D. C., Lipsky, J. J. & Naylor, S. Determination of *in vivo* adducts of disulfiram with mitochondrial aldehyde dehydrogenase. *Biochem. Pharmacol.* **61**, 537–545 (2001).
- Chen, D., Cui, Q. C., Yang, H. & Dou, Q. P. Disulfiram, a clinically used anti-alcoholism drug and copper-binding agent, induces apoptotic cell death in breast cancer cultures and xenografts via inhibition of the proteasome activity. *Cancer Res.* **66**, 10425–10433 (2006).
- Zha, J. *et al.* Disulfiram targeting lymphoid malignant cell lines via ROS–JNK activation as well as Nrf2 and NF- κ B pathway inhibition. *J. Transl. Med.* **12**, 163 (2014).
- Safi, R. *et al.* Copper signaling axis as a target for prostate cancer therapeutics. *Cancer Res.* **74**, 5819–5831 (2014).
- Liu, P. *et al.* Liposome encapsulated disulfiram inhibits NF- κ B pathway and targets breast cancer stem cells *in vitro* and *in vivo*. *Oncotarget* **5**, 7471–7485 (2014).
- Dufour, P. *et al.* Sodium dithiocarbamate as adjuvant immunotherapy for high risk breast cancer: a randomized study. *Biotherapy* **6**, 9–12 (1993).
- Yip, N. C. *et al.* Disulfiram modulated ROS–MAPK and NF- κ B pathways and targeted breast cancer cells with cancer stem cell-like properties. *Br. J. Cancer* **104**, 1564–1574 (2011).

12. Lövborg, H. *et al.* Inhibition of proteasome activity, nuclear factor- κ B translocation and cell survival by the anti-alcoholism drug disulfiram. *Int. J. Cancer* **118**, 1577–1580 (2006).
13. Allensworth, J. L. *et al.* Disulfiram (DSF) acts as a copper ionophore to induce copper-dependent oxidative stress and mediate anti-tumor efficacy in inflammatory breast cancer. *Mol. Oncol.* **9**, 1155–1168 (2015).
14. Nechushtan, H. *et al.* A phase IIb trial assessing the addition of disulfiram to chemotherapy for the treatment of metastatic non-small cell lung cancer. *Oncologist* **20**, 366–367 (2015).
15. Jin, M. *et al.* Alcohol drinking and all cancer mortality: a meta-analysis. *Ann. Oncol.* **24**, 807–816 (2013).
16. Li, Y. *et al.* Copper improves the anti-angiogenic activity of disulfiram through the EGFR/Src/VEGF pathway in gliomas. *Cancer Lett.* **369**, 86–96 (2015).
17. Suzuki, Y. *et al.* The origin of an EPR signal observed in dithiocarbamate-loaded tissues. Copper(II)-dithiocarbamate complexes account for the narrow hyperfine lines. *Biochim. Biophys. Acta* **1335**, 242–245 (1997).
18. Kepp, O., Galluzzi, L., Lipinski, M., Yuan, J. & Kroemer, G. Cell death assays for drug discovery. *Nat. Rev. Drug Discov.* **10**, 221–237 (2011).
19. Doil, C. *et al.* RNF168 binds and amplifies ubiquitin conjugates on damaged chromosomes to allow accumulation of repair proteins. *Cell* **136**, 435–446 (2009).
20. Li, J. M., Wu, H., Zhang, W., Blackburn, M. R. & Jin, J. The p97-UFD1L-NPL4 protein complex mediates cytokine-induced κ B α proteolysis. *Mol. Cell. Biol.* **34**, 335–347 (2014).
21. Chou, T. F. & Deshaies, R. J. Quantitative cell-based protein degradation assays to identify and classify drugs that target the ubiquitin–proteasome system. *J. Biol. Chem.* **286**, 16546–16554 (2011).
22. Kisselev, A. F. & Goldberg, A. L. Monitoring activity and inhibition of 26S proteasomes with fluorogenic peptide substrates. *Methods Enzymol.* **398**, 364–378 (2005).
23. Asher, G., Lotem, J., Cohen, B., Sachs, L. & Shaul, Y. Regulation of p53 stability and p53-dependent apoptosis by NADH quinone oxidoreductase 1. *Proc. Natl Acad. Sci. USA* **98**, 1188–1193 (2001).
24. Asher, G., Tsvetkov, P., Kahana, C. & Shaul, Y. A mechanism of ubiquitin-independent proteasomal degradation of the tumor suppressors p53 and p73. *Genes Dev.* **19**, 316–321 (2005).
25. Verma, R. *et al.* Role of Rpn11 metalloprotease in deubiquitination and degradation by the 26S proteasome. *Science* **298**, 611–615 (2002).
26. Dai, R. M. & Li, C. C. Valosin-containing protein is a multi-ubiquitin chain-targeting factor required in ubiquitin–proteasome degradation. *Nat. Cell Biol.* **3**, 740–744 (2001).
27. Alexandru, G. *et al.* UBXD7 binds multiple ubiquitin ligases and implicates p97 in HIF1 α turnover. *Cell* **134**, 804–816 (2008).
28. Chou, T. F. *et al.* Reversible inhibitor of p97, DBeQ, impairs both ubiquitin-dependent and autophagic protein clearance pathways. *Proc. Natl Acad. Sci. USA* **108**, 4834–4839 (2011).
29. Riemer, A. *et al.* The p97-Ufd1-Npl4 ATPase complex ensures robustness of the G2/M checkpoint by facilitating CDC25A degradation. *Cell Cycle* **13**, 919–927 (2014).
30. Radhakrishnan, S. K., den Besten, W. & Deshaies, R. J. p97-dependent retrotranslocation and proteolytic processing govern formation of active Nrf1 upon proteasome inhibition. *eLife* **3**, e01856 (2014).
31. Meyer, H., Bug, M. & Bremer, S. Emerging functions of the VCP/p97 AAA-ATPase in the ubiquitin system. *Nat. Cell Biol.* **14**, 117–123 (2012).
32. Magnaghi, P. *et al.* Covalent and allosteric inhibitors of the ATPase VCP/p97 induce cancer cell death. *Nat. Chem. Biol.* **9**, 548–556 (2013).
33. Samali, A., Fitzgerald, U., Deegan, S. & Gupta, S. Methods for monitoring endoplasmic reticulum stress and the unfolded protein response. *Int. J. Cell Biol.* **2010**, 830307 (2010).
34. Auner, H. W. *et al.* Combined inhibition of p97 and the proteasome causes lethal disruption of the secretory apparatus in multiple myeloma cells. *PLoS ONE* **8**, e74415 (2013).
35. Soriano, G. P. *et al.* Proteasome inhibitor-adapted myeloma cells are largely independent from proteasome activity and show complex proteomic changes, in particular in redox and energy metabolism. *Leukemia* **30**, 2198–2207 (2016).
36. Lass, A., McConnell, E., Fleck, K., Palamarchuk, A. & Wójcik, C. Analysis of Npl4 deletion mutants in mammalian cells unravels new Ufd1-interacting motifs and suggests a regulatory role of Npl4 in ERAD. *Exp. Cell Res.* **314**, 2715–2723 (2008).
37. Voráčková, I., Suchanová, S., Ulbrich, P., Diehl, W. E. & Ruml, T. Purification of proteins containing zinc finger domains using immobilized metal ion affinity chromatography. *Protein Expr. Purif.* **79**, 88–95 (2011).
38. Holdgate, G. *et al.* Biophysical methods in drug discovery from small molecule to pharmaceutical. *Methods Mol. Biol.* **1008**, 327–355 (2013).
39. Lomenick, B. *et al.* Target identification using drug affinity responsive target stability (DARTS). *Proc. Natl Acad. Sci. USA* **106**, 21984–21989 (2009).
40. Becker, L. A. *et al.* Therapeutic reduction of ataxin-2 extends lifespan and reduces pathology in TDP-43 mice. *Nature* **544**, 367–371 (2017).
41. Guo, L. *et al.* A cellular system that degrades misfolded proteins and protects against neurodegeneration. *Mol. Cell* **55**, 15–30 (2014).
42. Kim, Y. E., Hipp, M. S., Bracher, A., Hayer-Hartl, M. & Hartl, F. U. Molecular chaperone functions in protein folding and proteostasis. *Annu. Rev. Biochem.* **82**, 323–355 (2013).
43. Dai, C. & Sampson, S. B. HSF1: guardian of proteostasis in cancer. *Trends Cell Biol.* **26**, 17–28 (2016).
44. Cvek, B. Targeting malignancies with disulfiram (Antabuse): multidrug resistance, angiogenesis, and proteasome. *Curr. Cancer Drug Targets* **11**, 332–337 (2011).
45. Deshaies, R. J. Proteotoxic crisis, the ubiquitin–proteasome system, and cancer therapy. *BMC Biol.* **12**, 94 (2014).
46. Anderson, D. J. *et al.* Targeting the AAA ATPase p97 as an approach to treat cancer through disruption of protein homeostasis. *Cancer Cell* **28**, 653–665 (2015).
47. Cui, Y. *et al.* High expression of valosin-containing protein predicts poor prognosis in patients with breast carcinoma. *Tumour Biol.* **36**, 9919–9927 (2015).
48. Yamamoto, S. *et al.* Expression of valosin-containing protein in colorectal carcinomas as a predictor for disease recurrence and prognosis. *Clin. Cancer Res.* **10**, 651–657 (2004).
49. Tsujimoto, Y. *et al.* Elevated expression of valosin-containing protein (p97) is associated with poor prognosis of prostate cancer. *Clin. Cancer Res.* **10**, 3007–3012 (2004).

Supplementary Information is available in the online version of the paper.

Acknowledgements We thank J. Škvor, M. Zadinová, J. Večerka and D. Doležal for help with animal experiments, Jana Vrbkova for statistical analysis, D. Fridecky and T. Adam for help with HPLC, I. Protivankova and M. Grønngvig Nielsen for technical assistance. This work was supported by grants from the Kellner Family Foundation, Czech National Program of Sustainability, Grant Agency of the Czech Republic, MEYS CR project Czech-Biomed, the Czech Health Research Council, of the Danish Cancer Society, the Danish National Research Foundation (project CARD), the Danish Council for Independent Research, the Novo Nordisk Foundation, the Czech Cancer League, the Swedish Research Council, Cancerfonden of Sweden, the European Commission (EATRIS), the Czech Ministry of Education, youth and sports (OPVKCZ), Cancer Research Czech Republic and the Howard Hughes Medical Institute.

Author Contributions Z.S., M.Mis., B.C., R.J.D. and J.Barte. conceived the study. Z.S. and M.Mis. performed most biochemical and microscopy experiments and wrote the manuscript. D.M. established the expression cell lines and performed most cytotoxicity tests. T.O., P.D. and I.V. performed the HPLC experiments. K.K.A., S.F. and J.O. performed the epidemiological analyses. J.Bartk. performed the immunohistochemical analyses. J.V. and P.D. performed DARTS experiments. P.M. performed cell death analyses. Z.T. performed cytotoxicity tests and heat-shock response analyses. A.K. performed cytotoxicity tests. A.M. designed and performed phlebotomies of patients treated with Antabuse. M.Mic. performed the ITC. J.G. performed FACS analyses, cell death assays and cell sorting. J.S. performed 20S proteasome assays. J.L. performed 26S proteasome assays. M.K. and C.D. performed the cytotoxicity experiments on myeloid- and patient-derived cell lines. P.P., J.M. and M.H. performed mouse experiments. J.Barte., B.C., Q.P.D. and R.J.D. helped to design the experiments, interpreted the data and wrote/edited the manuscript. All authors approved the manuscript.

Author Information Reprints and permissions information is available at www.nature.com/reprints. The authors declare competing financial interests: details are available in the online version of the paper. Readers are welcome to comment on the online version of the paper. Publisher's note: Springer Nature remains neutral with regard to jurisdictional claims in published maps and institutional affiliations. Correspondence and requests for materials should be addressed to J.Barte. (jb@cancer.dk), B.C. (cvek@seznam.cz) and R.J.D. (deshaies@caltech.edu).

Reviewer Information Nature thanks P. Brossart and the other anonymous reviewer(s) for their contribution to the peer review of this work.

METHODS

The experiments were not randomized.

Epidemiological analyses and access to health registers. We conducted a population-based cohort study by combining Danish nationwide demographic and health registers. This study was approved by the Danish Data Protection Agency and Statistics Denmark's Scientific Board. As the epidemiological study was based solely on register data and did not involve any contact with patients, no ethical approval was required from the Danish Scientific Ethical Committee⁵⁰. The cohort consisted of all Danes aged 35–85 years with a first-time diagnosis of cancer between January 2000 and December 2013. Because DSF (Antabuse) is a relative contra-indication among individuals with liver or kidney diseases, we excluded patients with cancers of the liver or kidney from the cohort. Cohort members were categorized according to use of DSF into two main groups: (i) those who filled at least one prescription of DSF within five years before the cancer diagnosis, but did not fill DSF prescription(s) during the first year after the diagnosis (previous users), that is, individuals suffering from alcoholism but taking DSF only before their cancer diagnosis; and (ii) those who used DSF before their cancer diagnosis and also filled one or more DSF prescriptions during the first year after the cancer diagnosis (continuing users), that is, individuals who underwent DSF therapy both before and after the cancer diagnosis. We also defined a category of patients with cancer who did not fill prescription(s) for DSF either before or after (≤ 1 year) the cancer diagnosis (never users). In the main analyses, we calculated hazard ratios and 95% confidence intervals estimating cancer-specific mortality among continuing DSF users compared to previous DSF users based on a Cox model regressing on both propensity scores and disulfiram use. By including propensity scores in the regression, we used demographic data and comorbid conditions/diagnostic codes as well as prescription data for selected concomitant drugs, to balance baseline characteristics of previous and continuing users of DSF and to adjust estimated hazard ratios of cancer-specific mortality associated with DSF use⁵¹. The patients with cancer were followed from one year after the diagnosis until death, migration or end of study (31 December 2014). The propensity scores thus estimate the probability of being treated with DSF in the exposure window 0–1 year after the cancer diagnoses conditional on the following other covariates in the calculation of propensity scores using logistic regression: gender, age at diagnosis, calendar time, highest achieved education and disposable income; medical histories of diabetes mellitus, chronic obstructive pulmonary disease, ischaemic heart disease, congestive heart failure, cerebrovascular disease, atrial fibrillation or atrial flutter, dementia and ulcer disease; and use of non-steroidal anti-inflammatory drugs (NSAIDs; including aspirin), non-aspirin antithrombotic agents (anticoagulants), statins, antihypertensive medication, other cardiovascular drugs, anti-diabetics and psychotropic drugs. In the Cox model, the propensity score is further included as a restricted cubic spline to model possible nonlinearities, in addition to the categorical disulfiram use, which is the variable of interest. Analyses were run for cancer overall and for breast, prostate and colon cancer, separately. Furthermore, all analyses were stratified by stage (localized, non-localized or unknown). Statistical significance of DSF use was evaluated by likelihood ratio tests. We used the software R for statistical computing⁵².

In vivo tumour experiments. The human breast cancer cell line MDA-MB-231 was injected (10^7 cells transplanted subcutaneously) to grow tumours in athymic NU/NU female mice (AnLab Ltd) with a body weight of 23.6–26.9 g, aged 12 weeks. Inclusion criteria were: female, appropriate age and weight (15–30 g). Exclusion criteria were: tumour size must not exceed 20 mm (volume 4,000 mm³) in any direction in an adult mouse, the tumour mass should not proceed to the point where it significantly interferes with normal bodily functions, or causes pain or distress owing to its location, persistent self-induced trauma, rapid or progressive weight loss of more than 25%, for seven days. In none of the experiments were these approved ethical limits exceeded. After the tumours grew to 0.114–0.117 cm³ on average, mice were randomly divided into four groups, each of eight mice, and treated as follows: (i) normal diet; (ii) normal diet plus oral administration of 0.15 mg kg⁻¹ copper gluconate (CuGlu); (iii) normal diet plus oral administration of 50 mg kg⁻¹ DSF; (iv) normal diet plus oral administration of 0.15 mg kg⁻¹ CuGlu and 50 mg kg⁻¹ DSF. Administration of compounds was carried out as a blinded experiment (all information about the expected outputs and the nature of used compounds were kept from the animal technicians). CuGlu was administered each day in the morning (08:00) and DSF each day in the evening (19:00) to mimic a clinical trial combining DSF and CuGlu in treatment of tumours involving the liver (NCT00742911). After treatment began, mice were weighed and their tumours measured twice per week. At day 32, mice were euthanized, and the tumours were removed and frozen at -80°C . The experiment was evaluated by comparing growth curves of tumours in the experimental groups with those in controls. The rates of tumour growth inhibition (TGI) were calculated by the formula $\text{TGI} = (1 - V_{\text{treated}}/V_{\text{control}})$ where V_{treated} is the mean of tumour volumes in the treated group and V_{control} is the mean of tumour volumes in the control group.

Mean tumour volume values at specific time intervals were statistically evaluated. To test directly the effect of CuET, we used MDA-MB-231 and AMO-1 models. MDA-MB-231 was injected (5×10^6 cells were transplanted subcutaneously) to grow tumours in SCID mice (ENVIGO) aged 10 weeks (± 2 weeks). AMO-1 xenografts were expanded in SCID mice. Each group consisted of 10 animals, each bearing two tumours. CuET was formulated in bovine serum albumin solution (1%) to a final concentration of 1 mg ml⁻¹. CuET was applied intraperitoneally with a schedule of five days on and two days off. All aspects of the animal study met the accepted criteria for the care and experimental use of laboratory animals, and protocols were approved by the Animal Research Committee of the 1st Faculty of Medicine Charles University in Prague and Ethical Committee of Faculty of Medicine and Dentistry, Palacky University in Olomouc. For HPLC-MS and immunohistochemistry analysis, we used MDA-MB-231 xenografted mice treated with the same DSF and DSF plus copper gluconate regime as described for the anti-cancer activity assessment with the notable difference that mice were euthanized after five days of treatment.

HPLC-MS analysis of CuET. The HR-MRM analysis was performed on a HPLC-ESI-QTOF system consisting of HPLC chromatograph Thermo UltiMate 3000 with AB Sciex TripleTOF 5600+ mass spectrometer, using the DuoSpray ESI source operated at an ion source voltage of 5,500 V, ion source gas flow rates of 40 units, curtain gas flow rate of 30 units, declustering potential of 100 V and temperature 400 °C. Data were acquired in product ion mode with two parent masses (358.9 and 360.9) for analysis of CuET. Chromatographic separation was done by PTFE column, which was especially designed for analysis of strong metal chelators filled by C18 sorbent (IntellMed, IM_301). Analysis was performed at room temperature and with a flow rate of 1,500 $\mu\text{l min}^{-1}$ with isocratic chromatography. Mobile phase consisted of HPLC grade acetone (Lachner) 99.9%, HPLC water (Merck Millipore) 0.1% and 0.03% HPLC formic acid (Sigma-Aldrich). Acquired mass spectra were evaluated in software PeakView 1.2. Extracted ion chromatograms of transitions 88.0 and 116.0 (common for both parent masses) with a 0.1 mass tolerance were Gaussian smoothed with width of two points. Peak area was then recorded and recalculated to ng ml⁻¹ according to the calibration curve.

Sample preparation for HPLC-MS analysis. Liquid nitrogen-frozen biological samples were cut into small pieces using a scalpel. Samples (30–100 mg) were immediately processed by homogenization in 100% acetone in a ratio of 1:10 sample:acetone (for plasma or serum the ratio was 1:4). Homogenization was done in a table-top homogenizer (Retsch MM301) placed in a cold room (4 °C) in 2-ml Eppendorf tubes with 2 glass balls (5 mm) for 1 min at 30 Hz. The tube was immediately centrifuged at 4 °C, 20,000g for 2 min. Supernatant was decanted into a new 1.5-ml Eppendorf tube and immediately centrifuged for 30 min using a small table-top centrifuge (BioSan FVL-2400N) placed inside a -80°C freezer. Supernatant was quickly decanted into a glass HPLC vial and kept at -80°C for no longer than 6 h. Just before the HPLC analysis, the vial was placed into a pre-cooled (4 °C) LC-sample rack and immediately analysed. To enable an approximate quantification of analysed CuET, a calibration curve was prepared. Various amounts of CuET were spiked in plasma, frozen in liquid nitrogen, and placed at -80°C to mimic sample processing. Standards were then processed as the samples described above. To measure circulating CuET concentrations, mice were given a single oral dose of DSF (50 mg kg⁻¹) and euthanized at different time points. Serum was collected and frozen for analysis.

Blood collection from humans for HPLC-MS analysis of CuET. Blood samples were collected before and 3 h after oral application of DSF (Antabuse, 400 mg) dissolved in water. Phlebotomy needles were specific for metal analysis—Sarstedt Safety Kanule 21G \times 1½ inches, 85.1162.600. Collection tubes were specific for metal analysis—Sarstedt, S-Monovette 7.5 ml LH, 01.1604.400. Immediately after blood collection samples were centrifuged in a pre-cooled centrifuge (4 °C at 1,300g for 10 min). After centrifugation, tubes were placed on ice and the plasma fraction was immediately aliquoted into the 1.5-ml Eppendorf tubes with approximately 500 μl per tube. The tubes with plasma were immediately frozen on dry ice and later stored in -80°C . Blood samples were collected from volunteers who gave informed consent and were undergoing Antabuse therapy because of alcohol abuse. Participants were four males (aged 34, 38, 41, 60 years) and five females (aged 37, 56, 46, 59, 63 years). All individuals were freshly diagnosed for alcohol-use disorder and were scheduled for Antabuse therapy. Blood samples were collected before and after the first use of Antabuse. All relevant ethical regulations were followed for the study. The study, including the collection of blood samples, was approved by the Ethical Committee of Faculty of Medicine and Dentistry, Palacky University in Olomouc.

Cell lines. Cell lines were cultured in appropriate growth medium supplemented with 10% fetal bovine serum (FBS) and penicillin–streptomycin; and maintained in a humidified, 5% CO₂ atmosphere at 37 °C. Cell lines cultured in DMEM medium were: HCT116 (ATCC), DU145 (ECACC), PC3 (ECACC), T47D (NCI60),

HS578T (NCI60), MCF7 (ECACC), MDA-MB-231 (ATCC), U2OS (ECACC), HeLa (ATCC), NIH-3T3 (ATCC), CAPAN-1 (ATCC), A253 (ATCC), FaDu (ATCC), h-TERT-RPE1 (ATCC), HeLa-Ub(G76V)-GFP-ODD-Luc²¹. Cell lines cultured in RPMI1640 medium were: NCI-H358 (ATCC), NCI-H52 (ATCC), HCT-15 (ATCC), AMO-1 (ATCC), MM-1S (ATCC), ARH77 (ATCC), RPMI8226 (ATCC), OVCAR-3 (NCI60), CCRF-CEM (ATCC), K562 (ATCC), 786-0 (NCI60). Cell lines cultured in EMEM medium were: U87-MG (ATCC), SiHA (ATCC). Cell line A549 (ATCC) was cultured in F12K medium, HT29 (ATCC) in McCoy's medium and LAPC4 (provided by Z. Culig, University of Innsbruck) in IMDM medium supplemented with metribolone R1881 (Sigma-Aldrich). RWPE-1 (ATCC) cells were cultured in a keratinocyte serum-free medium supplemented with bovine pituitary extract and human recombinant epidermal growth factor (Thermo Fisher Scientific). BTZ- and CFZ-resistant multiple myeloma cell lines were previously described in ref. 35. Cell lines were tested for mycoplasma contamination and authenticated by STR method. None of the cell lines used in this study is listed in the database of commonly misidentified cell lines maintained by ICLAC.

Stable cell line construction. For construction of all stably transfected cell lines we used the U2OS cell line (ECACC). For U2OS Ub-GFP, we used the commercial Ub-GFP EGFP-C1 vector (Addgene); for U2OS NPL4-GFP, we used the commercial NPLOC4-GFP pCMV6-AC-GFP vector (Origene); for U2OS p97-GFP, we used the commercial VCP-GFP pCMV6-AC-GFP vector (Origene); and for U2OS UFD1-GFP, we used the commercial UFD1L-GFP pCMV6-AC-GFP vector (Origene). Cells were transfected using Promega FugeneHD according to the manufacturer's instructions. Cells were further cultured in the appropriate antibiotics (geneticin, 400 µg ml⁻¹). Medium with geneticin was replaced every 2–3 days until the population of resistant cells was fully established. Cells were further refined by sorting for cells expressing GFP (BD FACS Aria). For preparation of inducible NPL4(MUT)-GFP cells, U2OS cells were transfected with a pcDNA6/TR plasmid (Invitrogen, V1025-20) using the FugeneHD transfection reagent (Promega, E2311) according to the manufacturer's protocol. To generate a cell line that stably expressed the Tet repressor, U2OS cells were cultured in selective medium with blasticidin (10 µg ml⁻¹) for 10 days. Blasticidin-resistant colonies were picked, expanded and screened for clones that exhibited the lowest basal levels and highest inducible levels of expression. Next, the most suitable clones were transfected with the PCDNA4/TO expression vector encoding the mutated NPL4-GFP protein using the Fugene transfection reagent. Cells were cultured in medium with zeocin (500 µg ml⁻¹) to select clones that contain pcDNA4/TO-mutated NPL4-GFP. The NPL4(MUT)-GFP-encoding plasmid was obtained from Geneti Biotech. To induce expression of protein, cells were incubated with doxycycline (Sigma-Aldrich) 1 µg ml⁻¹ for 16–48 h.

Colony-formation assay. Cells were seeded into six-well plates at 100–300 cells per well (depending on the cell line). The next day, cells were treated with compounds as indicated in the specific experiments and kept in culture for 7–14 days. Colonies were visualized by crystal violet and counted.

XTT assay. Cells were plated at a density of 10,000 per well in a 96-well plate. The next day, cells were treated as indicated. After 24 h, an XTT assay was performed according to the manufacturer's instructions (Applchem). XTT solution was added to the medium and incubated for 30–60 min, and then the dye intensity was measured at the 475 nm wavelength using a spectrometer (TECAN, Infinite M200PRO). Results are shown as mean ± s.d. from three independent experiments, each performed in triplicate. For LD₅₀ analysis across the panel of cell lines listed in Extended Data Fig. 2b, cell lines were treated with various doses (at least five doses) for 48 h. LD₅₀ values were calculated using Graphpad Prism software based on survival curves from at least two independent experiments.

Annexin V staining. Cell cultures were treated as indicated and collected by trypsinization. Initial culture medium and washing buffer were collected to include detached cells. Cells were centrifuged (250g, 5 min) and re-suspended in a staining buffer (140 mM NaCl, 4 mM KCl, 0.75 mM MgCl₂, 10 mM HEPES) containing 2.5 mM CaCl₂, Annexin-V-APC (1:20, BD Biosciences) and 2.5 µg ml⁻¹ 7-AAD (BD Biosciences) for 15 min on ice in the dark. Samples were analysed by flow cytometry using BD FACSSuite (BD Biosciences) and at least 10,000 events were acquired per sample. Collected data were processed using BD FACSSuite (BD Biosciences) and exported into Microsoft Excel.

Caspases 3/7 assay. Activity of caspase-3 and -7 was quantified by cleavage of fluorogenic substrate CellEvent Caspase-3/7 Green Detection Reagent (Thermo Fisher Scientific). In brief, samples prepared in the same staining buffer as described for annexin V staining above, supplemented with 2% FBS, 0.5 µM CellEvent Caspase-3/7 Green Detection Reagent and incubated for 45 min at room temperature in the dark. Subsequently, 0.5 µg ml⁻¹ DAPI was added and samples were analysed by flow cytometry using BD FACSSuite (BD Biosciences) and at least 10,000 events were acquired per sample. Collected data were processed using BD FACSSuite (BD Biosciences) and exported into Microsoft Excel.

Viability assay of multiple myeloma cells. The CellTiter 96 MTS-assay (Promega) was used according to the manufacturer's instructions to determine the cell viability of BTZ (Janssen Cilag), CFZ and CuEt in cell lines and the absorbance of the formazan product was measured in 96-well microplates at 492 nm. The assay measures dehydrogenase enzyme activity found in metabolically active cells.

For patient cells, the more sensitive luminescent CellTiterGlo assay (Promega) was used to determine cell viability, measured by ATP production of metabolically active cells. The primary myeloma cell samples were obtained after written informed consent and approval by the independent ethics review board (St Gallen ethics committee—Ethikkommission Ostschweiz), in accordance with ICH-GCP and local regulations. Malignant plasma cells were retrieved by PBMC isolation from a patient with multiple myeloma progressing under BTZ-containing therapy, based on IMWG criteria (BTZ-resistant) and an untreated patient with multiple myeloma (BTZ-sensitive). The purity of the cell samples was >80% myeloma cells, as assessed by morphology.

Immunoblotting and antibodies. Equal amounts of cell lysates were separated by SDS-PAGE on hand-cast or precast tris-glycine gradient (4–20%) gels (Life Technologies), and then transferred onto a nitrocellulose membrane. The membrane was blocked with 5% bovine milk in Tris-buffered saline containing 0.1% Tween-20 for 1 h at room temperature, and then incubated overnight at 4 °C or for 1 h at room temperature, with one of the following primary antibodies (all antibodies were used in the system under study (assay and species) according to the instructions of the manufacturer): anti-ubiquitin (1:1,000; Cell Signaling, 3933), anti-H2A, acidic patch (1:1,000; Merck Millipore, 07-146), anti-monoubiquityl-H2A (1:1,000; Merck Millipore, clone E6C5), anti-IκBα (1:500; Santa Cruz Biotechnology, sc-371), anti-p53 (1:500; Santa Cruz Biotechnology, clone DO-1), anti-HIF-1α (1:1,000; BD Biosciences, 610958), anti-CDC25A (1:500; Santa Cruz Biotechnology, clone DCS-120), anti-NRF1 (1:1,000; Cell Signaling, clone D5B10), anti-VCP (1:2,000; Abcam, ab11433), anti-VCP (1:1,000; Novus Bio, NBP100-1557), anti-NPLOC4 (1:1,000; Novus Bio, NBP1-82166), anti-ubiquitin lys48-specific (1:1,000; Merck Millipore, clone Apu2), anti-β-actin (1:2,000; Santa Cruz Biotechnology, sc-1616; or 1:500; Santa Cruz Biotechnology, sc-87778), anti-GAPDH (1:1,000; GeneTex, clone 1D4), anti-lamin B (1:1,000; Santa Cruz Biotechnology, sc-6217), anti-calnexin (1:500; Santa Cruz Biotechnology, sc-11397), anti-α-tubulin (1:500; Santa Cruz Biotechnology, sc-5286), anti-XBP1 (1:500; Santa Cruz Biotechnology, sc-7160), UFD1 (1:500; Abcam, ab155003), cleaved PARP1 (1:500; Cell Signaling, 9544), p-eIF2α (1:500; Cell Signaling, 3597), ATF4 (1:500; Merck Millipore, ABE387), HSP90 (1:500; Enzo, ADI-SPA-810), HSP70 (1:500; Enzo, ADI-SPA-830), HSF1 (1:500; Cell Signaling, 4356), p-HSP27 (1:1,000; Abcam, 155987), HSP27 (1:1,000; Abcam, 109376) followed by detection by secondary antibodies: goat anti-mouse IgG-HRP (GE Healthcare), goat anti-rabbit (GE Healthcare), donkey anti-goat IgG-HRP (Santa Cruz Biotechnology, sc-2020). Bound secondary antibodies were visualized by ELC detection reagent (Thermo Fisher Scientific) and images were recorded by imaging system equipped with CCD camera (ChemiDoc, Bio-Rad) operated by Image Laboratory software or developed on film (Amersham).

Immunofluorescence staining. Cells were grown in 24-well plates with a 0.170-mm glass bottom (In Vitro Scientific). Where indicated, the cells were pre-extracted before fixation with pre-extraction buffer (10 mM PIPES pH 6.8, 100 mM NaCl, 1.5 mM MgCl₂, 300 mM sucrose, 0.5% Triton X-100, 1 mM DTT, 5 µg ml⁻¹ leupeptin, 2 µg ml⁻¹ aprotinin, 0.1 mM PMSF) for 20 min at 4 °C, washed by PBS and then immediately fixed with 4% formaldehyde for 15 min at room temperature. Cells were stained with primary antibodies: anti-ubiquitylated conjugated mouse FK2 antibody (1:500; Enzo, BML-PW8810), anti-VCP (1:500; Abcam; ab11433), anti-NPL4 (1:500; Novus Bio, NBP1-82166), HSP70 (1:100; Enzo, ADI-SPA-830), HSF1 (1:500; Cell Signaling, 4356), anti-ubiquitin lys48-specific (1:500; Merck Millipore, clone Apu2), SUMO2/3 (1:500; Abcam, ab3742), TDP43 (1:300; Proteintech, 10782-2-AP) and appropriate Alexa Fluor 488 and 568-conjugated secondary antibodies (Invitrogen, 1:1,000). Cytochrome *c* was stained using an Alexa Fluor 555-conjugated mouse anti-cytochrome *c* antibody according to the manufacturer's protocol (BD Pharmingen, 558700).

Microscopy, FRAP and image analysis. Samples were analysed using a Zeiss Axiomager Z.1 platform equipped with the Elyra PS.1 super-resolution module for structured illumination (SIM) and the LSM780 module for CLSM. High resolution images were acquired in super-resolution mode using a Zeiss Pln Apo100×/1.46 oil objective (total magnification, 1,600×) with appropriate oil (Immersol 518F). SR-SIM setup involved five rotations and five phases for each image layer and up to seven z-stacks (101 nm) were acquired per image. The CLSM setup for FRAP and life cells acquisition had a c-Apo 40×/1.2 W water immersion objective. Bleaching of regions of interest (ROIs) was performed using an Argon 488 nm laser. Lower resolution images of fixed samples were acquired using a Plan Apo 63×/1.4 oil objective (total magnification 1,008×). FRAP and image acquisitions were performed using Zeiss Zen 11 software. For FRAP, internal Zen's 'Bleach'

and 'Regions' modules were used. Data from FRAP analysis involving multiple bleached ROIs were exported into Microsoft Excel and plotted. Basic processing of acquired images, such as contrast and brightness settings, was done in Adobe Photoshop on images exported as TIFFs. Quantitative microscopy-based cytometry of the immunofluorescence-stained samples was performed using an automatic inverted fluorescence microscope BX71 (Olympus) using ScanR Acquisition software (Olympus) and analysed with ScanR Analysis software (Olympus).

Cell fractionation for Triton-X100 insoluble pellets. Cells were treated as indicated, washed in cold PBS and lysed in lysis buffer (50 mM HEPES pH 7.4, 150 mM NaCl, 2 mM MgCl₂, 10% glycerol, 0.5% Triton X-100, protease inhibitor cocktail by Roche) for 10 min gently agitating at 4°C. Then, cells were scraped into Eppendorf tubes and kept for another 10 min on ice with intermittent vortexing. After that, the lysate was centrifuged at 20,000g for 10 min at 4°C. The insoluble fraction and supernatant were separately re-suspended in 1 × LSB buffer.

Isolation of microsomal fraction. After the desired treatment in cell culture, cells were washed with cold PBS and lysed (250 mM sucrose, 20 mM HEPES pH 7.4, 10 mM KCl, 1.5 mM MgCl₂, 1 mM EDTA, 1 mM DTT, protease inhibitor cocktail). Lysates were homogenized by Potter-Elvehjem PTFE homogenizer and kept on ice for 20 min. The homogenates were subjected to serial centrifugation steps (720g and 10,000g for 5 min each, and 100,000g for 1 h). Pellets and supernatants from the last ultracentrifugation step were resuspended in the 1 × LSB buffer and used for western blot analysis.

Immunoperoxidase staining of pre-extracted tissue sections. Frozen sections (4–5 μm thick) from xenograft-grown, cryopreserved tumour tissues were cut on a cryostat and placed on commercial adhesion slides (SuperFrost Plus, Menzel, Germany) and air-dried for 2 h at room temperature. The dried sections were carefully covered with the cold extraction buffer: 50 mM Tris-HCl (pH 7.5), 150 mM NaCl, 1 mM MgCl₂, 5% glycerol, 1 mM DTT, 1% Triton X-100, 1% IGEAL, protease inhibitor cocktail (Phos Stop Easy pack, 04906837001, Roche) or cold PBS (controls) and incubated in a cold room for 20 min. Pre-extracted and control PBS-treated sections were gently washed three times in cold PBS, and fixed in 4% paraformaldehyde fixative for 15 min, followed by another three washes in PBS. Washed sections were then subject to a sensitive immunoperoxidase staining protocol, using the primary rabbit monoclonal antibody against VCP antibody (EPR3307(2)) (1:10,000; ab109240, Abcam) and rabbit polyclonal antibody against NPLOC4 (1:500; NBP1-82166, Novus Biologicals) and Vectastain Elite kit as secondary reagents (Vector Laboratories, USA), followed by a nickel-sulfate-enhanced diaminobenzidine reaction without nuclear counterstaining, mounted and microscopically evaluated and representative images documented by an experienced oncopathologist.

Isothermal titration calorimetry (ITC). Experiments were performed at 25°C with a Nano ITC Low Volume (TA Instruments) and analysed by Nano Analyze Software v.2.3.6. During all measurements, injections of 2.5 μl of ligand (16 μM) were titrated into 250 μl protein (2 μM) with time intervals of 300 s, a stirring speed of 250 r.p.m. All ITC experiments were conducted with degassed buffered solutions 20 mM HEPES buffer pH 7.3, in the presence of 1% DMSO. Purified GST-NPL4(WT) and GST-NPL4(MUT) proteins were used in ITC experiment.

Drug affinity responsive target stability (DARTS). DARTS was performed according to a modified published protocol³⁸. Purified GST-NPL4(WT) and GST-NPL4(MUT) proteins were diluted by 100 mM phosphate buffer, pH 7.4 to final concentration of 0.03 μg μl⁻¹. The proteins were treated with CuET (final concentration of 5 μM; dissolved in DMSO) for 1 h and equal amounts of DMSO were added to the solutions, which served as control samples. Pronase (Sigma-Aldrich) was dissolved in TNC buffer (50 mM Tris-Cl, 50 mM NaCl, 10 mM CaCl₂, pH 7.5). The 0.025 μg of pronase was added to 50 μl of protein solution and incubated for 1 h at 37°C. Samples without pronase served as the non-digested controls. The pronase reaction was stopped by addition of 5 × SDS loading buffer; the samples were boiled at 95°C for 15 min and loaded on SDS-PAGE gels. After SDS-PAGE, gels were silver-stained and scanned on a GS-800 Calibrated Densitometer (Bio-Rad) or used for western blot analysis.

20S proteasome activity. To measure proteasome activity in cell extracts, cell lines were seeded in 100-mm Petri dishes at a density of 3 × 10⁶ cells per dish. After 24 h, cells were washed twice with 2 ml of ice-cold PBS and scraped in to 1,000 μl ice-cold PBS. The cells were then isolated and suspended in buffer (50 mM HEPES (pH 7.5), 150 mM NaCl, 1% Triton X-100 and 0.1 μM PMSF) and then centrifuged at 15,000 r.p.m. for 15 min at 4°C. The cell lysates (10 μg) were incubated with 20 μM of substrates for measurement of chymotrypsin-like, trypsin-like and caspase-like activities (Suc-LLVT-AMC, Ac-RLR-AMC and Z-LLE-AMC (Boston Biochem)) in 90 μl of assay buffer (30 mM Tris-HCl, 0.035% sodium dodecylsulfate (pH 7.4)) in the presence CuET (1 μM and 5 μM) and BTZ (1 μM) for the investigation of proteasome inhibition; BTZ or an equivalent volume of solvent (DMSO) was used as a control. After 2 h of incubation at 37°C, inhibition of proteasome activity was measured by the release of hydrolysed free AMC groups by fluorimeter at

380/460 nm (TECAN, Infinite M200PRO). To measure proteasome activity in live cells, the cells were seeded in 24-well plate at a density of 0.2 × 10⁶ cells per well. Cell lines were treated with CuET (1 μM and 5 μM), vehicle control or 1 μM BTZ for 1 h. After incubation, cells were twice washed with 0.5 ml of 1 × ice-cold PBS and scraped into 100 μl ice-cold lysis buffer and then centrifuged at 15,000 r.p.m. for 15 min at 4°C. Subsequently, the cell extract (10 μg) was incubated with 20 μM substrates to measure chymotrypsin-like, trypsin-like and caspase-like activities in assay buffer (30 mM Tris-HCl (pH 7.4)). After 2 h of incubation at 37°C, inhibition of proteasome enzymatic activities was measured by the release of hydrolysed free AMC as described above.

Ub(G76V)-GFP degradation. HeLa Ub(G76V)-GFP-ODD-Luc cells expressing Ub(G76V)-GFP were seeded at a density of 10⁴ cells per well in 96-well plates. The next day, cells were treated with 4 μM MG132 for 3 h. After that, the medium was discarded and cells were washed twice with PBS and then incubated with the tested compound in the presence of 30 μg ml⁻¹ cycloheximide for another 3 h. The GFP signal was acquired using an ImageXpress automated microscope. For each well, four images were taken (corresponding to 200–250 cells). Cells were analysed every 30 min during 3 h of treatment. Normalized GFP signal intensity was calculated using the following formula: (test compound – background)/(basal GFP signal intensity × background) where 'test compound' is defined as the mean GFP signal intensity of Ub(G76V)-GFP-expressing cells treated with the test compound. 'Background' is defined as the background GFP signal intensity of HeLa cells. 'Basal GFP signal intensity' is defined as mean GFP signal intensity of Ub(G76V)-GFP-expressing cells treated with DMSO. The degradation rate constant (*k*) was obtained from the slope of the linear range of plotting ln(normalized GFP signal intensity) versus time ranging from 90 to 180 min. The percentage of remaining *k* for each compound is calculated using the following formula (test compound/DMSO control) × 100.

p97 ATPase activity assay. P97 ATPase assay was performed as described previously²⁸. A total of 250 nM of p97 protein was diluted in assay buffer (50 mM Tris-HCl pH 7.4, 20 mM MgCl₂, 0.5 mM DTT). Test compounds were added in DMSO (final concentration of DMSO was 5%). After 10 min of incubation, the reaction was started with ATP (100 μM final concentration) followed by a 1-h incubation at room temperature. The reaction was stopped by adding Biomol green solution (Enzo) and free phosphate was measured according to the manufacturer's instructions. Results are expressed as the percentage of activity of the control (a well containing only DMSO).

26S proteasome activity. The RPN11 assay is described in PubChem (AID588493). In brief, a synthetic fluorescently labelled substrate, Ub4pepOG, was used to measure RPN11 activity. Fluorescence polarization assay was performed in a low-volume 384-well solid black plate in the presence of (i) 5 μl of the compound 1,10-phenanthroline or CuEt in 3% DMSO or 3% DMSO control; (ii) 5 μl of BioMol 26S proteasome; and (iii) 5 μl of substrate (15 nM Ub4pepOG). Fluorescence polarization was measured using a plate reader with excitation of 480 nm and emission of 520 nm filter set. The activity was normalized to DMSO control and fit to a dose-response curve.

Protein expression and purification. All proteins were expressed in *E. coli* BL21 (DE3) cells (Novagen). p97-His (pET28a vector) and Ufd1-His (pET28a vector) expression were induced by 1 mM IPTG (Life Technologies) at an OD₆₀₀ of 0.6 for 10 h at 22°C. NPL4(WT) and NPL4(MUT) (pGEX-2TK) were induced by 0.4 mM IPTG at an OD₆₀₀ of 0.8 overnight at 16°C. For p97 and UFD1, the bacterial pellet was suspended in buffer (50 mM Tris-HCl pH 8.0, 300 mM NaCl, 2.5 mM MgCl₂, 20 mM imidazole, 5% glycerol) and lysed by sonication and centrifuged (14,000g for 20 min). Proteins were purified by Ni-NTA chromatography (Qiagen) according to the manufacturer's instructions. For p97, the protein was further purified by gel filtration (Superdex 200, GE Healthcare). For GST-NPL4(WT) and GST-NPL4(MUT), the bacterial pellet was suspended in phosphate buffer (PBS, 0.1% Triton X-100, 300 mM NaCl) and lysed by sonication and centrifuged (14,000g for 10 min). Proteins were purified by glutathione sepharose 4B (Life Technologies) according to the manufacturer's protocol. The proteins were further purified by gel filtration (Superdex 200, GE Healthcare).

Chemicals. CuET was prepared by direct synthesis from water solutions of diethyldithiocarbamate sodium salt and copper(II) chloride as described previously⁵³. CuET for *in vivo* experiments was prepared equally with a slight modification. The reaction between diethyldithiocarbamate sodium salt and copper(II) chloride was performed in a sterile 1% aqueous solution of bovine serum albumin. The resulting solution was used directly. The following chemicals were purchased from commercial vendors: tetraethylthiuram disulfide (disulfiram, DSF) (Sigma-Aldrich), sodium diethyldithiocarbamate trihydrate (Sigma-Aldrich), copper D-gluconate (Sigma-Aldrich), BTZ (Velcade, Janssen-Cilag International N.V.), MG132 (Sigma-Aldrich), DBE-Q (Sigma-Aldrich), NMS873 (Abmole), cycloheximide (Sigma-Aldrich), dicoumarol (Sigma-Aldrich), 1,10-phenanthroline (Sigma) and MLN7243 (Active Biochem).

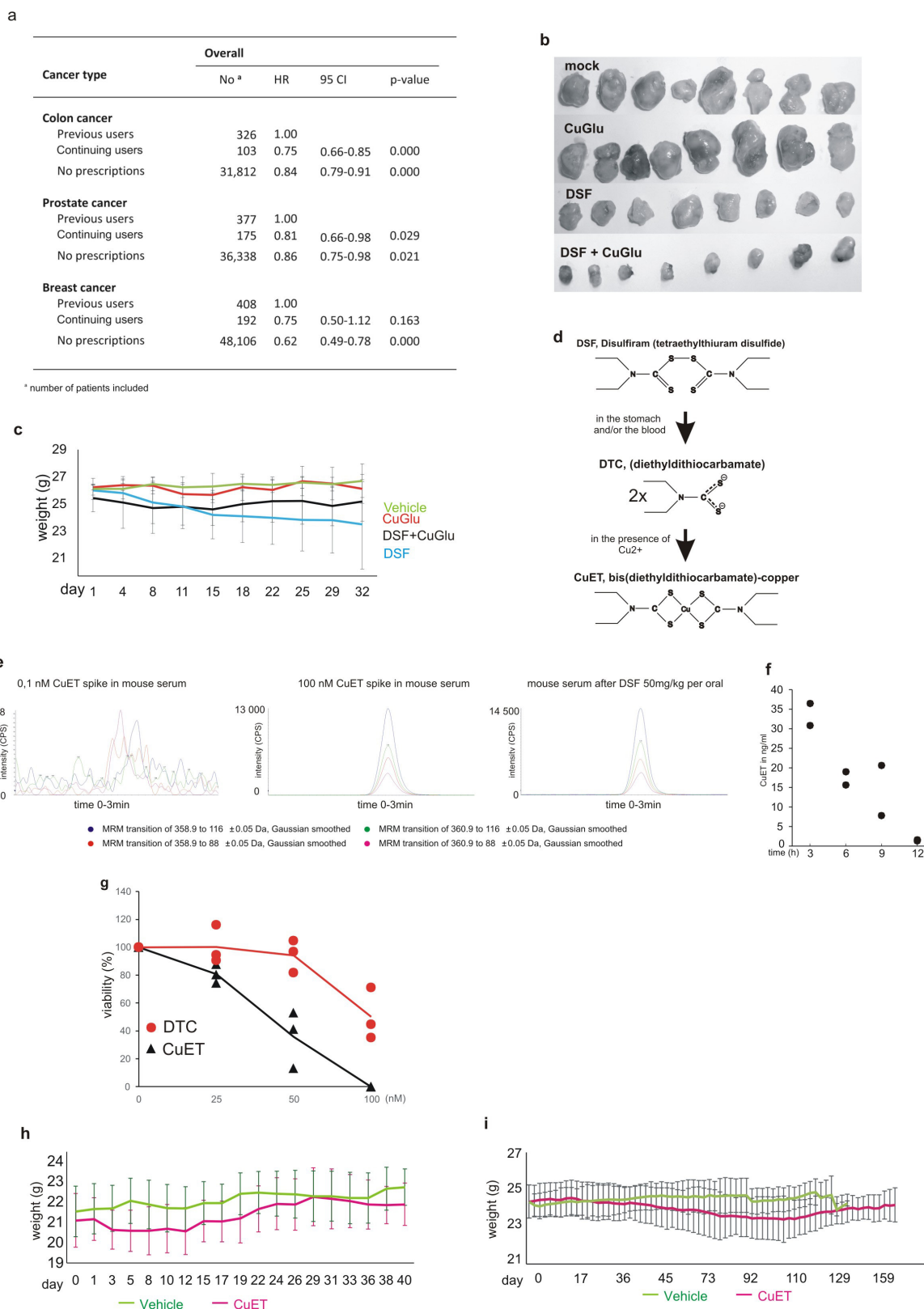
Statistical analyses and reproducibility. For the epidemiological study, we calculated hazard ratios and 95% confidence intervals estimating cancer-specific mortality, based on a Cox model regressing of both propensity scores and disulfiram use, balancing baseline characteristics of previous and continuing users of DSF and adjusting estimated hazard ratios of cancer-specific mortality associated with DSF use⁵¹. The propensity score estimates were conditional on multiple covariates, based on using logistic regression (see 'Epidemiological analyses and access to health registers' for specifics of cohorts and covariates). In the Cox model, the propensity score is further included as a restricted cubic spline to model possible nonlinearities, in addition to the categorical disulfiram use as the variable of interest. Statistical significance of DSF use was evaluated by likelihood ratio tests, using the software R for statistical computing⁵².

For evaluation of the animal studies, STATISTICA software, v.12 (StatSoft) was used to estimate sample size. For a power of 80%, the level of significance set at 5%, 4 groups and RMSSE = 0.8, seven mice per group were estimated. For usage of non-parametrical statistical methods, the number of eight mice per group was finally planned. The differences between tumour volumes were statistically analysed by non-parametrical Kruskal–Wallis test, not requiring any assumptions of normality and homoscedascity. To test the effect of CuET treatment on survival of AMO-1-xenografted mice, a Kaplan–Meier graph and log-rank statistical test were

used. For other experiments, the statistics, such as number of repetitions, centre value and error bars, are specified in figure legends.

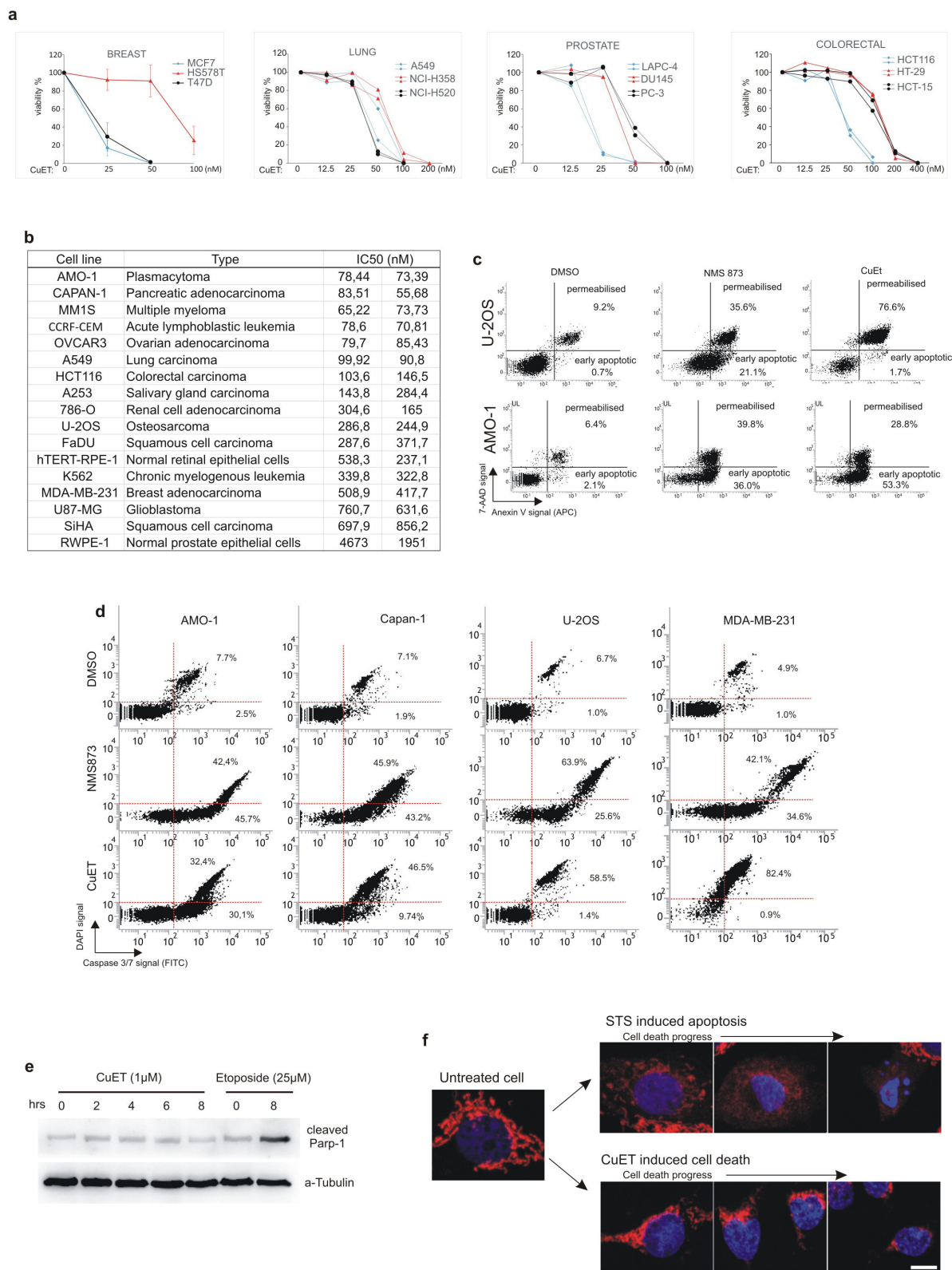
Data availability. Most data generated or analysed during this study are included in the article and its Supplementary Information. Uncropped images of all gels and blots can be found in Supplementary Fig. 1. Source Data for all graphs are provided in the online version of the paper. Additional datasets generated during and/or analysed during the current study and relevant information are available from the corresponding authors upon reasonable request.

50. Thygesen, L. C., Daasnes, C., Thaulow, I. & Brønnum-Hansen, H. Introduction to Danish (nationwide) registers on health and social issues: structure, access, legislation, and archiving. *Scand. J. Public Health* **39** (Suppl), 12–16 (2011).
51. Rosenbaum, P. R. & Rubin, D. B. The central role of the propensity score in observational studies for causal effects. *Biometrika* **70**, 41–55 (1983).
52. R Core Team. *R: A language and environment for statistical computing*. R Foundation for Statistical Computing <https://www.R-project.org/> R v.3.2.3 (2015-12-10) (R Foundation for Statistical Computing, 2016).
53. Cvek, B., Milacic, V., Taraba, J. & Dou, Q. P. Ni(II), Cu(II), and Zn(II) diethyldithiocarbamate complexes show various activities against the proteasome in breast cancer cells. *J. Med. Chem.* **51**, 6256–6258 (2008).



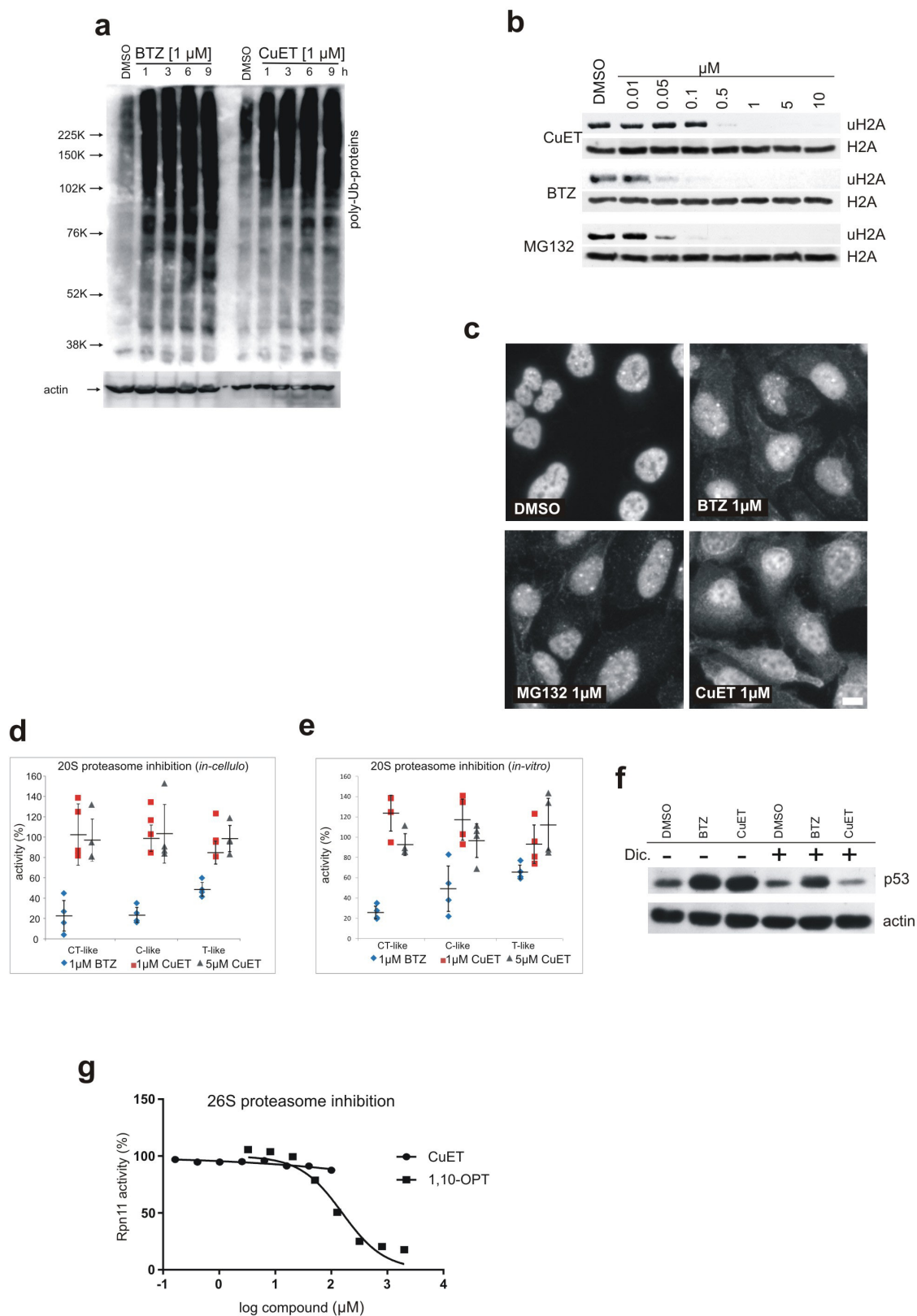
Extended Data Figure 1 | Epidemiological and pre-clinical data of the anti-cancer effects of DSF. **a**, Summary of hazard ratios (HR) and 95% confidence intervals (CI) for cancer-specific mortality among Danish patients with cancer, comparing continuing and previous users of DSF for selected types of cancer (for statistical analysis and definitions of DSF exposure categories, see Methods). **b**, Photographs of subcutaneously growing human MDA-MB-231 tumours extracted from mice at day 32. **c**, Time-course diagram of mouse weight. $n = 8$ animals per group. **d**, Model of CuET formation during metabolic processing of orally administered DSF in the human body. **e**, Examples of mass-spectrometry spectra of

CuET expressed as peaks of 4 MRM transitions in mouse serum after CuET spikes, compared to orally applied DSF (50 mg kg^{-1}). Data are representative of two independent experiments. **f**, Pharmacokinetic analysis of CuET levels in mouse serum after orally applied DSF (50 mg kg^{-1}). $n = 2$ animals per time point. **g**, Effect of DTC and CuET on MDA-MB-231 cells analysed by colony formation assay. $n = 3$ independent experiments. **h**, Time-course diagram of weight in CuET- and vehicle-treated mice. $n = 10$ animals per group. **i**, Extended time-course diagram of weight in CuET- and vehicle-treated mice. $n = 10$ animals per group. Data are mean \pm s.d. (**c**, **h**, **i**) or linked means (**g**).



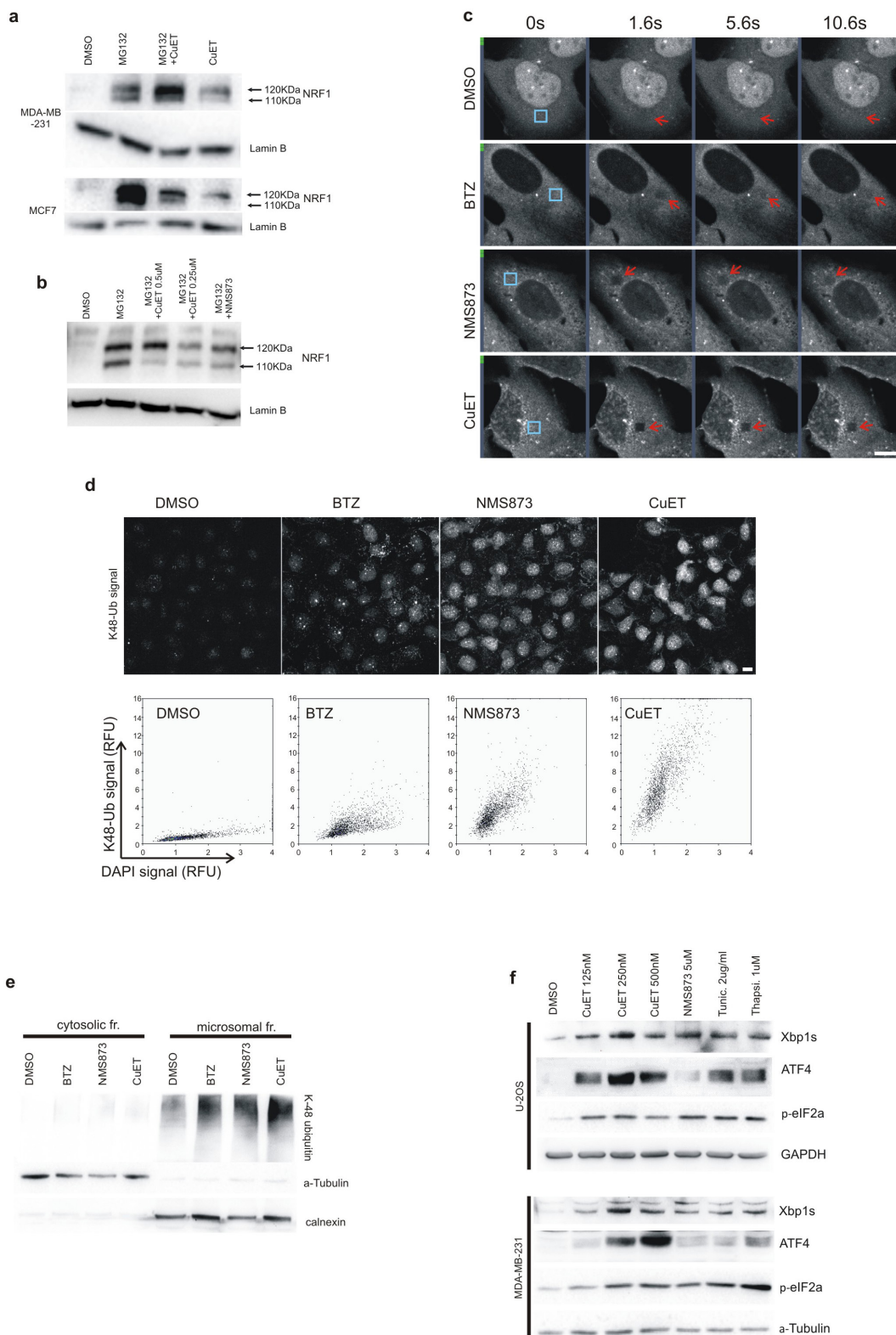
Extended Data Figure 2 | CuET is the major anti-cancer metabolite of DSF. **a**, CuET cytotoxicity measured by a colony-formation assay in human cell lines derived from breast, lung, colon and prostate carcinomas. Data are mean \pm s.d. of three independent experiments (breast) or presented individually for two independent biological experiments for each cell line (lung, colon and prostate). **b**, IC₅₀ values from two independent biological experiments documenting differential CuET-induced cytotoxicity across a panel of cancer and non-cancerous cell lines (48 h treatment). **c**, Analysis of annexin V signal in AMO-1 cells exposed to toxic doses of NMS873 (5 μ M, 16 h) or CuET (100 nM, 16 h) and in U2OS cell exposed to toxic doses of NMS873 (10 μ M, 16 h) or CuET

(1 μ M, 16 h). **d**, Analysis of caspase 3/7 activity in selected cell lines after apoptosis induction by NMS873 (AMO-1: 6 h, 5 μ M; Capan1: 16 h, 10 μ M; U2OS: 16 h, 10 μ M; MDA-MB-231: 24 h, 10 μ M) or CuET (AMO-1: 16 h, 100 nM; Capan1: 16 h, 250 nM; U2OS: 16 h, 1 μ M; MDA-MB-231: 24 h, 1 μ M). **e**, Absence of cleaved PARP1 after a toxic dose of CuET in U2OS cells, compared to etoposide treatment as a positive control. **f**, Analysis of cytochrome c (in red) release from mitochondria in U2OS cells during cell death induced by the positive control staurosporin (STS, 1 μ M) compared to cell death induced by CuET (1 μ M). Blue, DAPI. Scale bar, 10 μ m. **c-f**, Data are representative of two independent biological experiments.



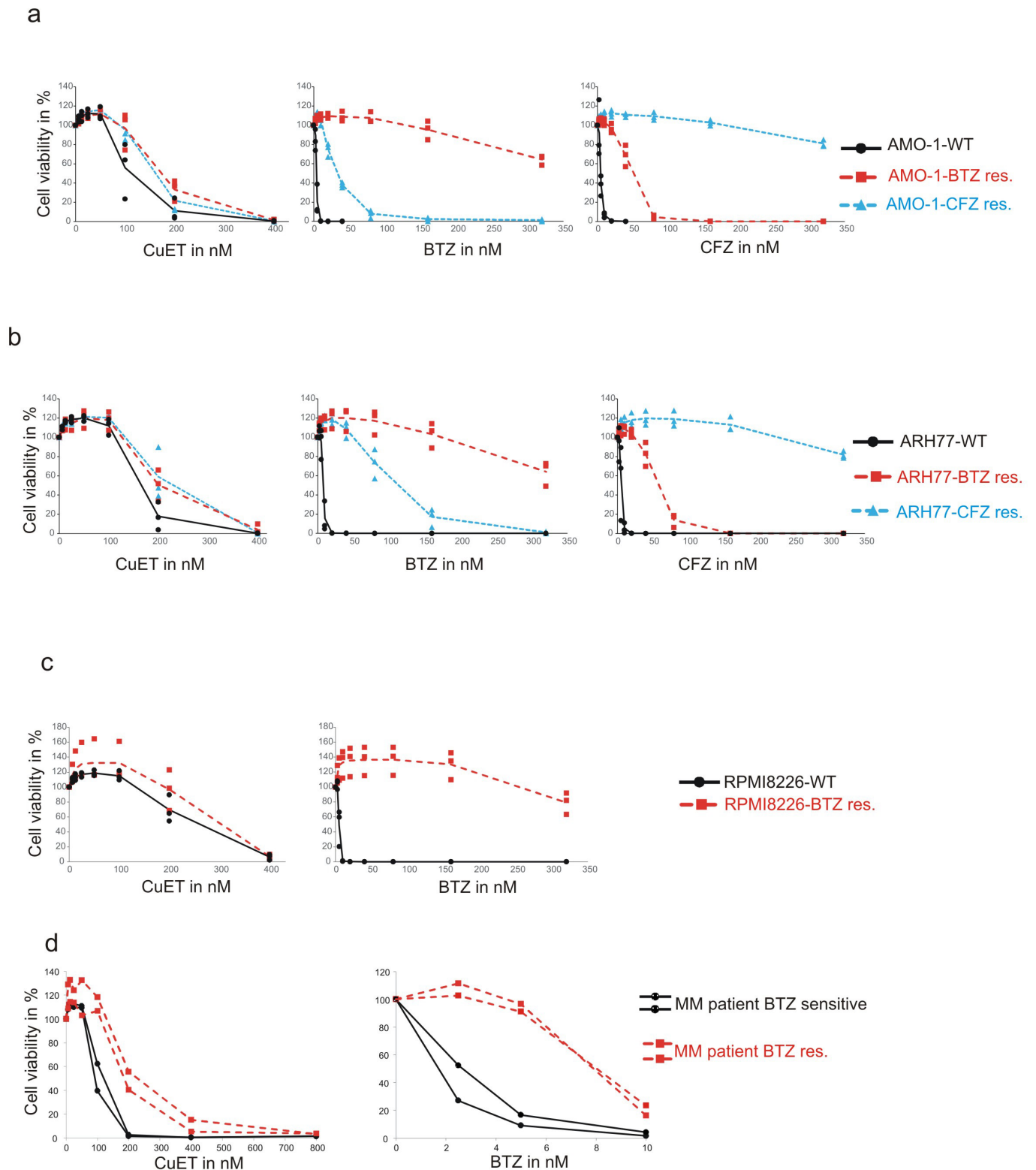
Extended Data Figure 3 | CuET-induced proteasome inhibition-like response is not due to proteasome inhibition. **a**, Kinetics of poly-Ub protein accumulation in U2OS cells treated with CuET or the proteasome inhibitor BTZ. **b**, CuET treatment (1.5 h) induces rapid deubiquitylation of ubiquitylated histone H2A (uH2A) similarly to proteasome inhibitors BTZ or MG132 in U2OS cells. **c**, CuET treatment (1.5 h) induces rapid cytoplasmic accumulation of poly-ubiquitylated proteins (FK2 antibody staining) in U2OS cells, similar to BTZ and MG132 treatment.

Scale bar, 10 μm . **d**, **e**, 20S proteasome activity is not inhibited by CuET as examined in live MDA-MB-231 cells (**d**) or in lysates from MDA-MB-231 cells (**e**). Data are mean \pm s.d. of four independent experiments. **f**, CuET treatment (1 μM , 6 h) does not cause accumulation of p53 in the presence of dicoumarol (300 μM) in MCF7 cells. **g**, *In vitro* 26S proteasome function measured as RPN11 deubiquitylation activity, is not inhibited by CuET; 1,10-phenanthroline (1,10-OPT) served as a positive control. Data are representative of two (**a–c**, **f**) or three (**g**) independent experiments.



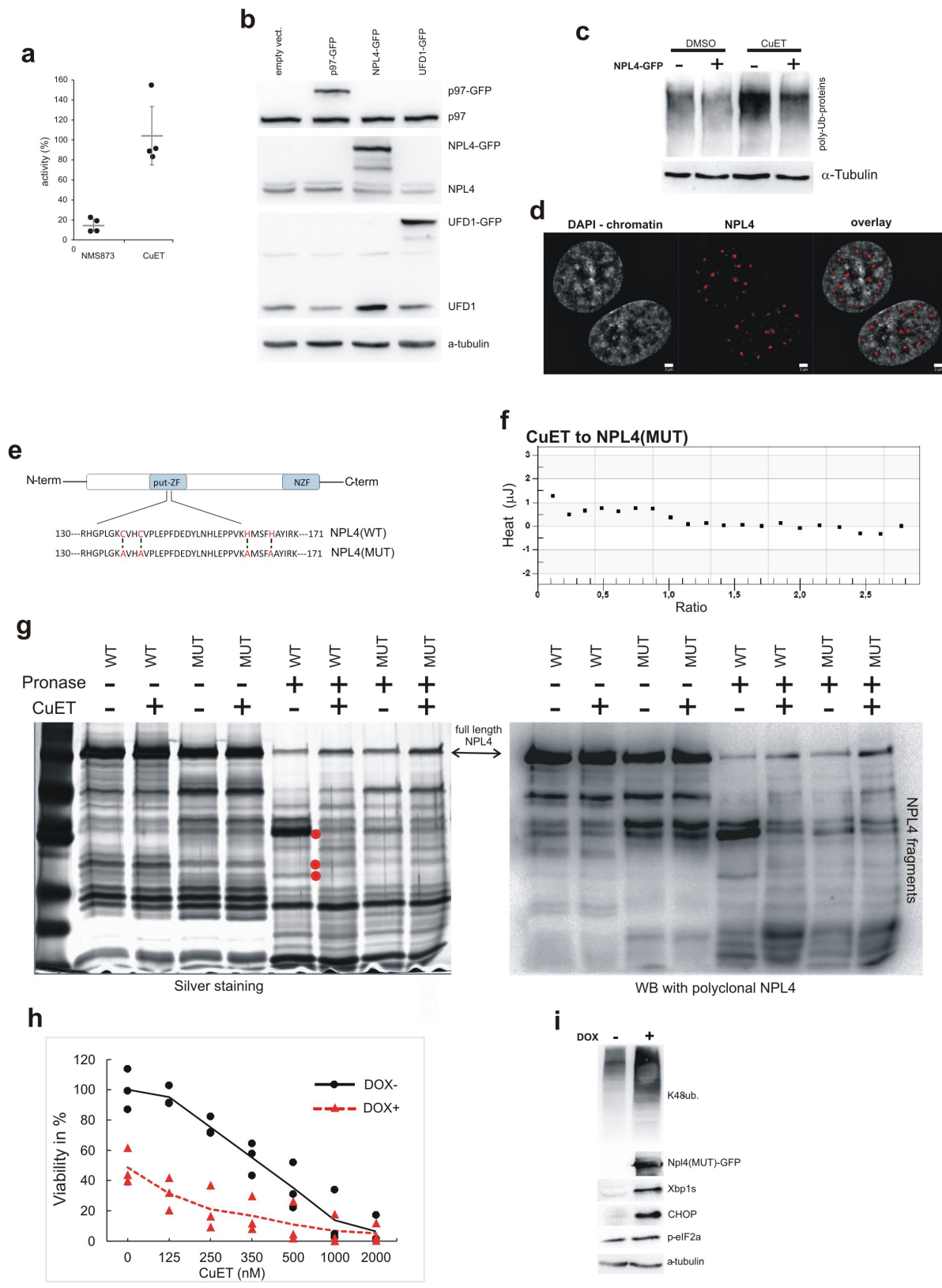
Extended Data Figure 4 | CuET inhibits the p97 pathway and induces cellular UPR. **a**, MG132-treated cells (5 μ M, 6 h) accumulate both forms of NRF1 (120-kDa and 110-kDa bands, top and bottom arrows, respectively), whereas CuET-treated cells (1 μ M, 6 h) accumulate only the non-cleaved 120-kDa form. **b**, Inhibition of the NRF1 cleavage process (appearance of the lower band) by CuET and NMS873 (a p97 inhibitor; 5 μ M) in mouse NIH3T3 cells co-treated with the proteasome inhibitor MG132 (5 μ M for 6 h). **c**, Time-course example images from a FRAP experiment, for which the quantitative analysis is shown in Fig. 2g (U2OS cells, blue boxes mark areas before bleaching, arrows after bleaching). **d**, U2OS cells pre-extracted with Triton X-100 and stained for poly-Ub(K48). The antibody

signal intensities for cells treated with DMSO, BTZ (1 μ M), NMS873 (10 μ M) and CuET (1 μ M) are analysed by microscopy-based cytometry and plotted below. **e**, Western blot analysis of accumulated poly-Ub proteins in the ultracentrifugation-separated microsomal fraction from U2OS cells treated with mock, CuET (1 μ M), NMS873 (10 μ M) or BTZ (1 μ M) for 3 h. **f**, UPR in U2OS and MDA-MB-231 cell lines induced by 6-h treatment with CuET (various concentrations) or positive controls (5 μ M NMS873, 2 μ g ml⁻¹ tunicamycin, 1 μ M thapsigargin) is shown by increased levels of XBP1s, ATF4 and p-eIF2 α . **a–f**, Data are representative of two independent experiments. All scale bars, 10 μ m.



Extended Data Figure 5 | CuET kills BTZ-resistant cells. **a**, BTZ-adapted (BTZres), CFZ-adapted (CFZres) and non-adapted AMO-1 human myeloma cells are equally sensitive to treatment with CuET. **b**, BTZ-adapted, CFZ-adapted and non-adapted ARH77 human plasmocytoma cells are equally sensitive to treatment with CuET. **c**, BTZ-adapted and non-adapted RPMI8226 human myeloma cells are equally sensitive to

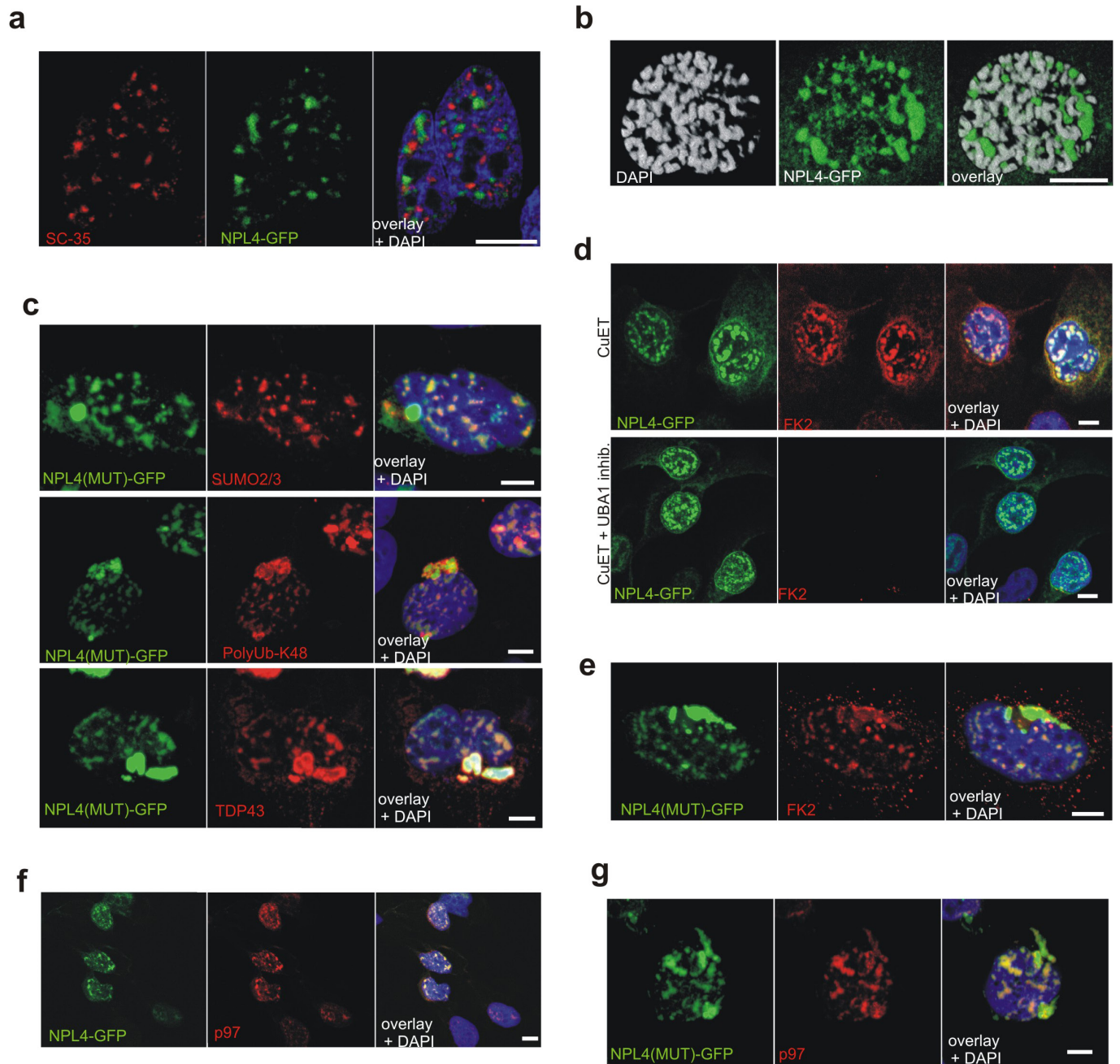
treatment with CuET. **d**, Human myeloma cells derived from a patient with BTZ-resistant myeloma show CuET sensitivity comparable to myeloma cells derived from a patient with BTZ-sensitive myeloma. Data are means linked of three independent experiments (a–c) or data are from two independent experiments (d).



Extended Data Figure 6 | See next page for caption.

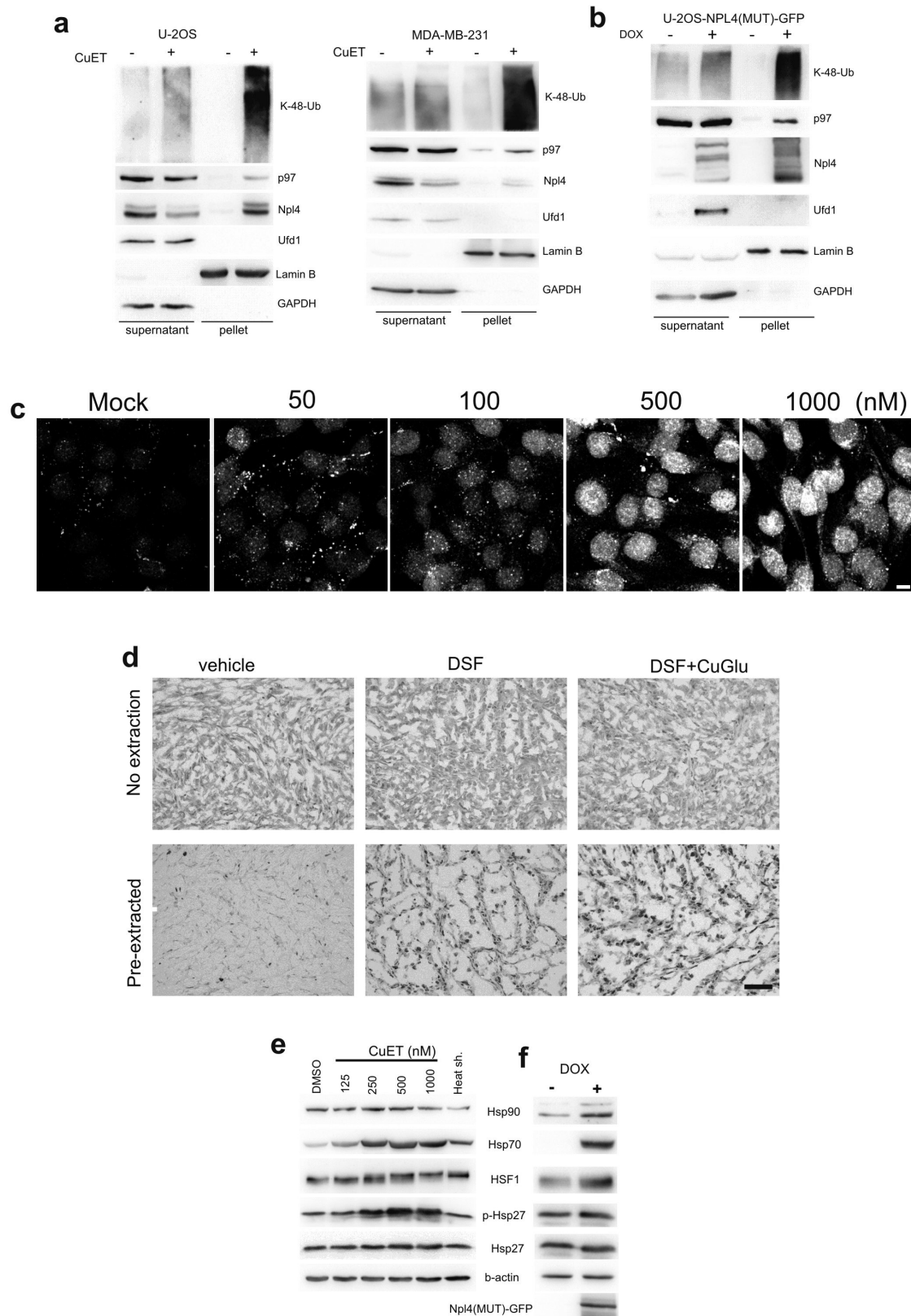
Extended Data Figure 6 | CuET targets NPL4, causing immobilization and nuclear clustering of NPL4. **a**, CuET (1 μ M) does not inhibit ATPase activity of p97. NMS873 (5 μ M) was used as a positive control. Data are mean \pm s.d. from four independent experiments. **b**, Western blotting analysis showing levels of ectopic p97-GFP, NPL4-GFP and UFD1-GFP in stable U2OS-derived cell lines used for the CuET-treatment rescue and cluster formation experiments. **c**, Ectopic expression of NPL4-GFP alleviates CuET-induced (125 nM, 4 h) accumulation of poly-Ub proteins in U2OS cells. **d**, Distribution of NPL4 nuclear clusters relative to chromatin in cells treated with CuET (1 μ M, 2 h). Scale bars, 2 μ m. **e**, Schematic representation of site-directed mutagenesis within the amino acid sequence of the putative zinc finger domain of NPL4.

f, ITC curve showing the lack of CuET binding to purified NPL4(MUT) protein. **g**, DARTS analysis of recombinant NPL4 proteins shows that differential pronase-mediated proteolysis after CuET addition is apparent for NPL4(WT) but not for NPL4(MUT); detected by either silver-stained SDS-PAGE (the most prominent differential bands are marked by red dots) or by blotting with an anti-NPL4 polyclonal antibody. **h**, Viability of cells expressing doxycycline-inducible NPL4(MUT)-GFP, treated with CuET for 48 h. Data are from three independent experiments, means are linked. **i**, Accumulation of K48-ubiquitinated proteins and activation of UPR in cells expressing the doxycycline-inducible NPL4(MUT)-GFP. **b-d**, **f**, **g**, **i**, Data are representative of two independent experiments.



Extended Data Figure 7 | Immobilized NPL4 forms insoluble protein aggregates. **a**, NPL4-GFP aggregates induced by CuET treatment (1 μ M, 3 h) do not co-localize with nuclear speckles (stained by SC-35 antibody) or nucleoli (visible as a DAPI⁻ nuclear signal). **b**, NPL4-GFP nuclear aggregates induced by CuET (1 μ M, 3 h) are excluded from chromatin in early prometaphase U2OS cells. **c**, Co-localization of spontaneous NPL4(MUT)-GFP aggregates with SUMO2/3, poly-UB(K48) and TDP43 in pre-extracted U2OS cells. **d**, NPL4-GFP aggregates are formed independently of ubiquitylation, as shown in CuET-treated (1 μ M, 3 h)

cells pre-treated with a chemical UBA1 inhibitor (MLN7243, 10 μ M, 1 h). The lack of cellular FK2 staining of ubiquitylated proteins validates the efficacy of the MLN7243 inhibitor. **e**, Co-localization of FK2 signal with the spontaneous NPL4(MUT)-GFP aggregates in pre-extracted U2OS cells. **f**, Analysis of p97 in CuET-induced (1 μ M, 3 h) NPL4-GFP aggregates in pre-extracted U2OS cells. **g**, Analysis of p97 in spontaneous NPL4(MUT)-GFP aggregates in pre-extracted U2OS cells. **a-g**, Data are representative of two independent biological experiments. All scale bars, 10 μ m.



Extended Data Figure 8 | NPL4 aggregation immobilizes the p97 binding partner and induces a global cellular HSR. **a**, Immobilization of selected proteins in Triton X-100-resistant pellet fractions of CuET-treated (1 µM, 3 h) U2OS cells. **b**, Immobilization of selected proteins in Triton X-100-resistant pellet fractions from U2OS cells expressing doxycycline-inducible NPL4(MUT)-GFP (48 h after induction). **c**, CuET dose-dependent immobilization of p97 in Triton X-100 pre-extracted MDA-MB-231 cells (3 h). Scale bar, 10µm. **d**, Immunohistochemical

staining showing non-extractable p97 in MDA-MB-231 xenografts from mice treated with DSF or DSF and CuGlu, compared to vehicle. Scale bar, 50µm. **e**, HSR after CuET (8 h treatment) is shown by various HSR markers detected by western blotting of U2OS cell extracts. **f**, HSR markers in U2OS cells expressing doxycycline-inducible NPL4(MUT)-GFP (24 h after induction). **a-f**, Data are representative of two independent biological experiments.

Life Sciences Reporting Summary

Nature Research wishes to improve the reproducibility of the work that we publish. This form is intended for publication with all accepted life science papers and provides structure for consistency and transparency in reporting. Every life science submission will use this form; some list items might not apply to an individual manuscript, but all fields must be completed for clarity.

For further information on the points included in this form, see [Reporting Life Sciences Research](#). For further information on Nature Research policies, including our [data availability policy](#), see [Authors & Referees](#) and the [Editorial Policy Checklist](#).

► Experimental design

1. Sample size

Describe how sample size was determined.

STATISTICA software, ver. 12 (StatSoft Inc., USA) was used to estimate the sample size. For the power of 80%, the level of significance set at 5%, 4 groups and RMSSE = 0.8, 7 mice in each group was estimated. For usage of non-parametrical statistical methods, the number of 8 (and 10) mice in each group was finally planned.

2. Data exclusions

Describe any data exclusions.

No data were excluded.

3. Replication

Describe whether the experimental findings were reliably reproduced.

All experiments were reproduced to reliably support conclusions stated in the manuscript.

4. Randomization

Describe how samples/organisms/participants were allocated into experimental groups.

Animals were randomly divided into experimental groups.

5. Blinding

Describe whether the investigators were blinded to group allocation during data collection and/or analysis.

Administration of compounds was carried out as a blinded experiment (all information about the expected outputs and the nature of used compounds were kept from the animal-technicians).

Note: all studies involving animals and/or human research participants must disclose whether blinding and randomization were used.

6. Statistical parameters

For all figures and tables that use statistical methods, confirm that the following items are present in relevant figure legends (or in the Methods section if additional space is needed).

- | n/a | Confirmed |
|-------------------------------------|-------------------------------------------------------------------------------------------------------------------------------------------------------------------------------------------------------------------------------|
| <input type="checkbox"/> | <input checked="" type="checkbox"/> The <u>exact sample size</u> (n) for each experimental group/condition, given as a discrete number and unit of measurement (animals, litters, cultures, etc.) |
| <input type="checkbox"/> | <input checked="" type="checkbox"/> A description of how samples were collected, noting whether measurements were taken from distinct samples or whether the same sample was measured repeatedly |
| <input type="checkbox"/> | <input checked="" type="checkbox"/> A statement indicating how many times each experiment was replicated |
| <input checked="" type="checkbox"/> | <input type="checkbox"/> The statistical test(s) used and whether they are one- or two-sided (note: only common tests should be described solely by name; more complex techniques should be described in the Methods section) |
| <input checked="" type="checkbox"/> | <input type="checkbox"/> A description of any assumptions or corrections, such as an adjustment for multiple comparisons |
| <input type="checkbox"/> | <input checked="" type="checkbox"/> The test results (e.g. P values) given as exact values whenever possible and with confidence intervals noted |
| <input type="checkbox"/> | <input checked="" type="checkbox"/> A clear description of statistics including <u>central tendency</u> (e.g. median, mean) and <u>variation</u> (e.g. standard deviation, interquartile range) |
| <input type="checkbox"/> | <input checked="" type="checkbox"/> Clearly defined error bars |

See the web collection on [statistics for biologists](#) for further resources and guidance.

► Software

Policy information about [availability of computer code](#)

7. Software

Describe the software used to analyze the data in this study.

The data were analyzed using Microsoft Excel 2016, STATISTICA 12, Graphpad Prism 4, PeakView 1.2, Image Lab 4.1, Carl Zeiss Zen 2011 SP6 (black), Nano Analyze Software 2.3.6, Olympus ScanR Analysis 1.3.0.3.

For manuscripts utilizing custom algorithms or software that are central to the paper but not yet described in the published literature, software must be made available to editors and reviewers upon request. We strongly encourage code deposition in a community repository (e.g. GitHub). *Nature Methods* [guidance for providing algorithms and software for publication](#) provides further information on this topic.

► Materials and reagents

Policy information about [availability of materials](#)

8. Materials availability

Indicate whether there are restrictions on availability of unique materials or if these materials are only available for distribution by a for-profit company.

All materials used is fully available from commercial sources with the exception of LAPC4 cell line, that we obtained from Zoran Culig, University of Innsbruck.

9. Antibodies

Describe the antibodies used and how they were validated for use in the system under study (i.e. assay and species).

anti-ubiquitin (Cell Signaling, cat.n.:3933; lot 4), anti-H2A, acidic patch (Merck Millipore, cat. n.: 07-146; lot 2880748), anti-monoubiquityl-H2A (Merck Millipore, clone E6C5; lot 2239798), anti-Ik β (Santa Cruz Biotechnology, cat. n.: sc-371), anti-phospho(Ser32/36)-Ik β (Cell Signaling, clone 5A5), anti-p53 (1:500; Santa Cruz Biotechnology, clone DO-1; D0915), anti-HIF1 α (BD Biosciences, cat. n.: 610958; lot 47858), anti-Cdc25A (Santa Cruz Biotechnology, clone DCS-120; our own clone commercially available by Santa Cruz), anti-NRF1 (Cell Signaling, clone D5B10; lot 1), anti-VCP (Abcam, cat. n.: ab11433; lot GR298429-3), anti-VCP (Novus Bio, cat. n.: NBP100-1557; lot A1), anti-NPLOC4 (Novus Bio, cat. n.: NBP1-82166; lot A96635), anti-ubiquitin lys48-specific (Merck Millipore, clone Apu2; lot 2724416), anti- β -actin (Santa Cruz Biotechnology, cat. n.: sc-1616; lot B2206), anti- β -actin (Santa Cruz Biotechnology, C4, cat. n.: sc-47778; lot C0916), anti-GAPDH (GeneTex, clone 1D4; lot 821603479), anti-Lamin B (Santa Cruz Biotechnology, M20, cat. n.: sc-6217; lot J2313), anti-calnexin (Santa Cruz Biotechnology, H70, cat. n.: sc-11397; lot C1214), anti- α -Tubulin (Santa Cruz Biotechnology, B7, cat. n.: sc-5286; lot C1313), anti-Xbp1 (Santa Cruz Biotechnology, M-186, cat. n.: sc-7160; lot A2314), CHOP (Cell Signaling, L63F7, cat. n.: 2895; lot 10), Ufd1 (Abcam, cat. n.: ab155003; lot GR119674-2), cleaved PARP1 (Cell Signaling, cat. n.: 9544; lot 4), p-eIF2 α (Cell Signaling, cat. n.: 3597; lot 9), ATF4 (Merck Millipore, cat. n.: ABE387 lot 2736396), HSP90 (Enzo, cat. n.: ADI-SPA-810; lot 05051501), TDP-43 (Proteintech, cat. n.: 10782-2-AP; lot number not provided by manufacturer), HSP70 (Enzo, cat. n.: ADI-SPA-830; lot 05021648), HSF1 (Cell Signaling, cat. n.: 4356; lot 2, pHSP27 (Abcam, cat. n.: 155987; lot GR117377), HSP27 (Abcam, cat. n.: 109376; lot GR61497-8). FK2 antibody (Enzo, cat. n.: BML-PW8810), Sumo2/3 (Abcam, cat. n.: ab3742; lot GR8249-1), Cytochrome c Alexa Fluor 555 conjugated (BD Pharmingen, cat. n.: 558700). Secondary antibodies: goat-anti mouse IgG-HRP (GE Healthcare), goat-anti rabbit (GE Healthcare), donkey-anti goat IgG-HRP (Santa Cruz Biotechnology, sc-2020), Alexa Fluor 488 and Alexa Fluor 568 (Invitrogen, 1:1000). Antibodies critical for novel conclusions were validated by elimination of signals upon KD experiments and/or by functional assays. All antibodies were used in the system under study (assay and species) according to the profile of manufacturer.

10. Eukaryotic cell lines

a. State the source of each eukaryotic cell line used.

HCT116 (ATCC), DU145 (ECACC), PC3 (ECACC), T47D (NCI60), HS578T (NCI60), MCF7 (ECACC), MDA-MB-231 (ATCC), U-2-OS (ECACC), HeLa (ATCC), NIH-3T3 (ATCC), CAPAN-1 (ATCC), A253 (ATCC), FaDu (ATCC), h-TERT-RPE1 (ATCC), NCI-H358 (ATCC), NCI-H52 (ATCC), HCT-15 (ATCC), AMO-1 (ATCC), MM-1S (ATCC), ARH77 (ATCC), RPMI8226 (ATCC), OVCAR-3 (NCI60), CCRF-CEM (ATCC), K562 (ATCC), 786-0 (NCI60), U87-MG (ATCC), SiHA (ATCC), A549 (ATCC), HT29 (ATCC), LAPC4 (kindly provided by prof. Zoran Culig, University of Innsbruck). RWPE-1 (ATCC)

b. Describe the method of cell line authentication used.

All cell lines authenticated by STR method.

c. Report whether the cell lines were tested for mycoplasma contamination.

All cell lines were tested for mycoplasma contamination.

d. If any of the cell lines used are listed in the database of commonly misidentified cell lines maintained by [ICLAC](#), provide a scientific rationale for their use.

None of the used cell lines is listed in ICLAC database.

► Animals and human research participants

Policy information about [studies involving animals](#); when reporting animal research, follow the [ARRIVE guidelines](#)

11. Description of research animals

Provide details on animals and/or animal-derived materials used in the study.

In this study were used athymic nu/nu female mice (AnLab Ltd.) median age 13 weeks (+/- 1 week) and SCID female mice (ENVIGO, NL) median age 10 weeks (+/- 2 weeks).

Policy information about [studies involving human research participants](#)

12. Description of human research participants

Describe the covariate-relevant population characteristics of the human research participants.

Human participants were 4 males (age of 34, 38, 41, 60 years) and 5 females (age of 37, 56, 46, 59, 63 years). All freshly diagnosed for alcohol use disorder and dedicated for Antabuse therapy. Blood samples were collected before and after first application of Antabuse.

Flow Cytometry Reporting Summary

Form fields will expand as needed. Please do not leave fields blank.

► Data presentation

For all flow cytometry data, confirm that:

- 1. The axis labels state the marker and fluorochrome used (e.g. CD4-FITC).
- 2. The axis scales are clearly visible. Include numbers along axes only for bottom left plot of group (a 'group' is an analysis of identical markers).
- 3. All plots are contour plots with outliers or pseudocolor plots.
- 4. A numerical value for number of cells or percentage (with statistics) is provided.

► Methodological details

5. Describe the sample preparation.

Cell cultures were treated as indicated and harvested by trypsinization. Initial culture medium and wash buffer were collected to include detached cells. Cells were centrifuged (250g, 5min) and resuspended in staining buffer (140 mM NaCl, 4 mM KCl, 0.75 mM MgCl₂, 10 mM HEPES). Then cell number was determined and after centrifugation, cells were resuspended in appropriate amount of staining buffer to get concentration of 1million cells per 900 microliters. For annexinV analysis, 1x10⁵ cells was incubated in 100 microliters of staining buffer containing 2.5 mM CaCl₂, Annexin V-APC (1:20, BD Biosciences) and 2.5 µg/ml 7-AAD (BD Biosciences) for 15 minutes on ice in the dark. For caspases 3/7 activity assay 1x10⁵ cells was incubated in 100 microliters of staining buffer supplemented with 2% FBS, 0.5 µM CellEvent™ Caspase-3/7 Green Detection Reagent (ThermoFisher Scientific) for 45 minutes at room temperature in the dark. Subsequently, 0.5 µg/mL DAPI was added before analysis by flow cytometry. Samples were analyzed by flow cytometry using BD FACSVersé (BD Biosciences), at least 10.000 events were acquired per sample . Collected data were processed by BD FACSSuite (BD Biosciences).

6. Identify the instrument used for data collection.

BD FACSVersé (BD Biosciences) equipped with 405nm,488nm and 640nm lasers, manufactured in october 2012.

7. Describe the software used to collect and analyze the flow cytometry data.

BD FACSSuite (BD Biosciences)

8. Describe the abundance of the relevant cell populations within post-sort fractions.

cell sorting not employed

9. Describe the gating strategy used.

Using the FSC/SSC gating, debris was removed by gating on the main cell population. Positivity threshold for each cell line was defined on the basis of mock-treated (DMSO) sample. Identical positivity threshold was applied to all samples within cell line.

Tick this box to confirm that a figure exemplifying the gating strategy is provided in the Supplementary Information.